# Coexistence of MORB- and OIB-like dolerite intrusions in the Purang ultramafic massif, SW Tibet: A paradigm of plume-influenced MOR-type magmatism prior to subduction initiation in the Neo-Tethyan lithospheric mantle

**Hao Zheng[1], Qiangtai Huang[1,†,§], Argyrios Kapsiotis[1], Davide Lenaz[2], Matteo Velicogna[2], Chi Xu[1], Chen Cheng[1], Bin Xia[1,†], Weiliang Liu[1], Yang Xiao[1], Peng Yang[1,3]**

[1]*Key Laboratory of Offshore Oil Exploration and Development of Guangdong Higher Education Institutes, Guangdong Provincial Key Laboratory of Marine Resources and Coastal Engineering, School of Marine Science, Sun Yat-sen University, Guangzhou 510275, China*

[2]*Department of Mathematics and Geosciences, University of Trieste, Via Weiss 8, Trieste 34128, Italy*

[3]*School of Earth and Environmental Sciences, The University of Queensland, Brisbane QLD 4072, Australia*

## ABSTRACT

**The Yarlung Zangbo Suture Zone (YZSZ) of South Tibet is divided by the Zhongba-Zhada terrane into two subparallel ophiolitic belts in its western end. The peridotite massifs of the southern belt tectonically overlie the Tethyan Himalaya sequence. The Purang peridotite body in this belt is intruded by two groups of dolerite dikes, providing significant compositional, geochronological, and isotopic information about the melting history of the Neo-Tethyan mantle. U-Pb ages of zircons separated from dolerites show that peridotites of West Purang were intruded by an early generation of dikes at 138.5 ± 2.0 Ma (Valanginian). These dolerites show ocean island basalt (OIB)-type normalized multi-elemental profiles and Sr-Nd isotopic signatures [$(La/Yb)_N$ = 13–16], high initial $^{87}Sr/^{86}Sr$ ratios (0.70598–0.70765), and low $\varepsilon_{Nd}(t)$ values (–2.6 to –2.3). Zircons separated from this group of dolerites have slightly radiogenic $\varepsilon_{Hf}(t)$ values (+2.6 to +4.6). The next generation of dolerite dikes intruded the East Purang peridotites between 124.5 ± 2.5 Ma and 124.4 ± 3.2 Ma (Aptian). These East Purang dolerites show normal mid-ocean ridge basalt (N-MORB)-type normalized multi-element patterns [$(La/Yb)_N$ = 0.6–0.9] with noticeable negative Nb and Th (±Ti) anomalies, and have high $^{87}Sr/^{86}Sr_{(i)}$ (0.70295–0.70618) and high $\varepsilon_{Nd}(t)$ values (+7.7 to +9.2). Zircons separated from the East Purang dolerites show strongly radiogenic $\varepsilon_{Hf}(t)$ values (+3.5 to +17.0).**

**Semiquantitative geochemical modeling demonstrates that the parental magmas of West Purang dolerites were generated from 5%–10% polybaric partial melting of a deep-seated juvenile asthenospheric source enriched by plume-type components. In contrast, the parental melts of East Purang dolerites were derived from more than 20% melting of a juvenile spinel-bearing MORB-type mantle source that was modified by subduction-related melts/fluids to a minor extent. A possible tectono-magmatic model for the petrogenesis of the Purang ophiolitic massif could be linked to incipient continental rifting and subsequent oceanic seafloor spreading associated with decompression upwelling of an asthenospheric source contaminated by plume-type components. This plume-proximal seafloor spreading-system was succeeded by the initiation of Neo-Tethyan intra-oceanic subduction close to the active continental margin of Eurasia during the Early Cretaceous.**

## INTRODUCTION AND RATIONALE OF THE STUDY

Ophiolites represent "fossil" sections of the Earth's old oceanic lithosphere that have been emplaced onto the continental crust (Anonymous, 1972). For this reason, ophiolites have been widely regarded as "natural laboratories" that can help us better understand intricate petrologic processes active within modern oceanic basins, arcs, and ocean-continent transitions (OCT), and also play a critical role in deciphering the mechanisms that build continental margins (e.g., Dilek and Furnes, 2011). For instance, accretion of ophiolites into continental margins due to competitive interaction between lithospheric plates is a first-order tectonic phenomenon contributing to the genesis of extensive mountain belts (e.g., Rassios and Dilek, 2009). The Alpine-Himalayan mountain range is probably the most typical paradigm of an ophiolite-bearing orogenic belt in the geological literature. This major suture zone was formed by the closure of the Neo-Tethys, a system of ocean basins that once existed between the ancient supercontinents of Gondwana and Laurasia during much of the Mesozoic era (Aitchison et al., 2000).

Important information is still missing about the complicated concept of the geodynamic configuration of the Neo-Tethys from its birth to its demise. Nevertheless, a great deal of practical and theoretical knowledge on this topic has been accumulated by a profusion of structural and petrologic studies of the Yarlung Zhangbo Suture Zone (YZSZ) ophiolites in South Tibet (China) over the last four decades (e.g., Nicolas et al., 1981; Allègre et al., 1984; Girardeau et al., 1985; Girardeau and Mercier, 1988; Pearce and Deng, 1988; Zhou et al., 1996, 2005; Wang et al., 2000; Hébert et al., 2003; Dupuis et al., 2005; Yang et al., 2007; Bédard et al., 2009; Wu et al., 2014; McGowan et al., 2015; Griffin et al., 2016; and references therein). Early models regarding the origin of the YZSZ ophiolites supported that they were generated at a slow-spreading mid-ocean ridge (MOR) similar to the present-day southwest Indian ridge (e.g., Nicolas et al., 1981; Girardeau and Mercier, 1988). However, the frequent occurrence of arc-type lavas in the crustal sequences of several ophiolites along the YZSZ implies that they were formed in a supra-subduction zone (SSZ)

†Corresponding authors.
§huangqt7@mail.sysu.edu.cn

setting (e.g., Wang et al., 2000; Hébert et al., 2003; Dubois-Côté et al., 2005; Dupuis et al., 2005; Zhou et al., 2005; Bédard et al., 2009) analogous to that below the Izu-Bonin-Mariana arc system (West Pacific).

Although the later model provides a meaningful solution to the so-called "global ophiolite conundrum" (SSZ-type ophiolites with MOR-type features; e.g., Moores et al., 2000), uncertainty regarding the true origin of the YZSZ ophiolites lingers due to the occasional discovery of extrusive and intrusive rocks with ocean island basalt (OIB)-like geochemical affinities in some of these ophiolites (e.g., Xia et al., 2008; Bézard et al., 2011; Dai et al., 2012; He et al., 2016). Such rocks have been interpreted as a result of adiabatic decompression melting of deep mantle ascending as asthenospheric diapir (Hébert et al., 2012) or through a lithospheric slab window (Dai et al., 2012). They have also been viewed as products of mixing of melts derived from variably depleted mantle sources beneath MOR settings (He et al., 2016). This diversity in genetic models demonstrates that our understanding of the origin of the OIB-type mafic rocks in the YZSZ ophiolites is still incomplete and that the mechanism controlling their formation may vary in several details among different ophiolites.

Herein, we report detailed geological, geochemical, and Sr-Nd isotopic data on the mafic (dolerite) dikes that intrude the Purang (/Yungbwa) ultramafic nappe (southwest YZSZ). We also report new U-Pb geochronological and Lu-Hf isotopic data for zircons separated from these mafic intrusions. Our data reveal important petrogenetic links between the extension of the lithospheric mantle and the intrusion of the mafic dikes that can aid in the resolution of the puzzling petrogenetic evolution of the Purang ophiolite.

## GEOLOGICAL SETTING

From north to south, the Tibetan Plateau (Fig. 1A) consists of the Songpan-Ganzi flysch complex, the eastern and western Qiangtang subterranes, the Lhasa terrane, and the Tethyan Himalaya sequence. These are separated by four long suture zones; namely, the Jinsha Suture Zone (JSSZ), Longmu Tso-Shuanghu Suture Zone (LSSZ), Bangong-Nujiang Suture Zone (BNSZ), and Yarlung Zangbo Suture Zone (YZSZ), all representing remnants of the vanished Tethyan Ocean (see Zhang et al., 2004 for a review).

In South Tibet, the continental collision between the northern passive margin of Greater India and the southern active continental margin of Eurasia resulted in the formation of the ~2000-km-long E-W–trending YZSZ (e.g., Aitchison et al., 2000; Fig. 1A). This major tectonic zone marks the terminal closure of the eastern branch of the Neo-Tethys in the broader Himalayan region (e.g., Hu et al., 2016 and references therein). The YZSZ separates the Gangdese magmatic arc (>150 Ma to 35 Ma) of the Lasha block to the north from the Tethyan Himalaya sequence to the south (e.g., Harrison et al., 2000; Chu et al., 2006, 2011; Wen et al., 2008; Ji et al., 2009; Li et al., 2018; and references therein; Fig. 1A). Scattered along the YZSZ is a discontinuous belt of ophiolites that are tectonically juxtaposed against accretionary prism complexes of the Mesozoic continental margin of Eurasia (e.g., Hébert et al., 2003; Fig. 1A).

The YZSZ is divided into three segments: the eastern segment that extends from Xigaze to the Eastern Himalaya syntaxis in the east. This segment has been strongly affected by N-S–oriented contractional deformation during and after the India-Asia collision (Xu et al., 2015). The central segment extends from Xigaze to Saga in the west. It is juxtaposed against the Cretaceous–Eocene Xigaze forearc basin sequence in the north, which does not exist in the other two segments of the YZSZ (e.g., Liu et al., 2018). The western segment extends from Saga to the Ladakh batholith in the NW and is divided, by the NW-SE–oriented ~900-km-long and ~100-km-wide Zhongba-Zhada terrane, into two structurally different belts known as the northern and southern belt (Fig. 1B). Ophiolites within the northern belt generally occur as discontinuous lensoidal bodies within a serpentinite matrix mélange. Major ophiolites within this belt include the Dajiweng, Baer, Cuobuzha, Gongzhu, and Saga peridotite massifs (Xia, 1991; Xia and Cao, 1992; Feng et al., 2015, 2017; Lian et al., 2016; Zheng et al., 2017; Liu et al., 2018). Ophiolites within the southern belt (i.e., Dongbo/Kiogar, Purang/Yungbwa, Xiugugabu, Dangqiong, Zhaga/South Gongzhucuo, Zhongba) are locally thrust northward onto the Zhongba-Zhada terrane, and southward onto the Tethyan Himalaya sequence (e.g., Liu et al., 2018 and references therein). The southwestern belt of the YZSZ is very important as it records all stages of the Wilson cycle (from continental rifting and seafloor spreading to slab subduction and collision) throughout the tectonic evolution of the Mesozoic Neo-Tethys.

### "Architecture" of the Purang Ophiolite

The Purang ophiolite crops out to the south of the YZSZ as a klippen massif (Searle et al., 1988; Hodges, 2000; Fig. 1C). It has a roughly NW-SE direction, covering a highly mountainous area of ~650 km$^2$ (Xu et al., 2011). It generally occurs as an ultramafic nappe overlying a Jurassic–Cretaceous volcanic-sedimentary sequence composed of massive basalt flows associated with radiolarites, siliceous to oolitic limestones, silty shales, and hydrothermally altered silicic tuffs (Huang et al., 2010; Liu et al., 2015a; Fig. 1C). This ultramafic nappe is dominated by variably depleted peridotites (Fig. 1C) occasionally hosting podiform chromitites (Xiong et al., 2018). Pyroxenite to gabbronorite intrusions and dolerite to basaltic dikes sporadically cross cut peridotites (Miller et al., 2003; Liu et al., 2015a). Ophicalcites made of angular serpentinite blocks, embedded in a calcite groundmass, are occasionally discernible within the Purang peridotites (Gansser, 1964). A poorly represented gabbroic sequence occupies the southeastern part of the ophiolitic massif (Fig. 1C). Unlike the ideal Penrose-type oceanic lithosphere Purang lacks a well-exposed sheeted dike complex. Furthermore, the absence of a sub-ophiolitic metamorphic sole indicates that the investigated ophiolite has been displaced by later fault movements, most likely in response to large-scale N-S shortening (Miller et al., 2003).

Bulk-rock geochronological dating of three basaltic intrusions in the Purang peridotites yielded a Sm-Nd isochron age of 147 ± 25 Ma, which is almost identical to the Ar-Ar age (152 ± 33 Ma) of amphibole (hornblende) separated from a basaltic intrusion (Miller et al., 2003). U-Pb dating of zircons separated from a gabbro intrusion and a gabbronorite dike within the Purang serpentinized harzburgites, using laser ablation–multi-collector–inductively coupled plasma–mass spectrometry (LA-MC-ICP-MS), yielded mean $^{206}Pb/^{238}U$ ages of 123.4 ± 0.8 Ma and 123.9 ± 0.9 Ma, respectively (Chan et al., 2015). In addition, U-Pb dating of zircons recovered from dolerite intrusions within the Purang peridotites using LA-ICP-MS yielded crystallization ages ranging from 130 Ma to 120 Ma (Li et al., 2008a; Liu et al., 2011).

The genesis of the Purang ophiolite is not fully understood yet. It has been viewed as: (*i*) a slice of MOR-type oceanic lithosphere (Miller et al., 2003) that was exhumed along a detachment fault at an ultra-slow spreading ridge setting (Liu et al., 2014), (*ii*) a continental margin-type ophiolite that was influenced by plume-type magmatism (Liu et al., 2015a), and (*iii*) a lithospheric slab that was initially formed in a MOR environment and then was modified by melts/fluids in a SSZ setting (Xu et al., 2008; Liu et al., 2015b; Su et al., 2015; Xiong et al., 2018). However, whole-rock Re-Os isotopic data indicate that peridotites in Purang are much older than their immediate crustal rocks (Liu et al., 2012; Gong et al., 2016) and most likely represent vestiges of old sub-continental lithospheric mantle (SCLM; Gong et al., 2016). Moreover, the discovery of ultra-high pressure

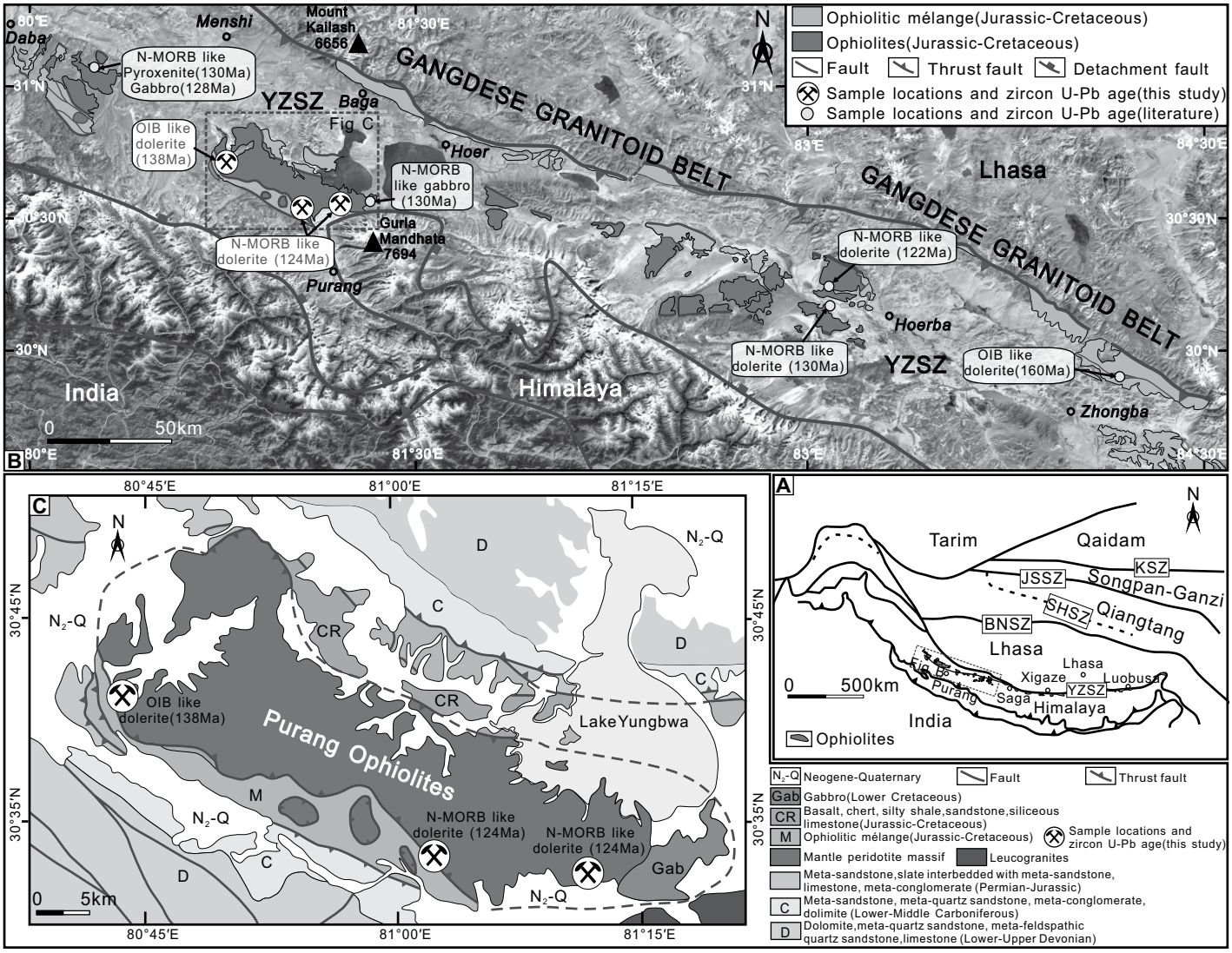


**Figure 1. (A) Schematic tectonic framework of the Tibetan Plateau (after Zhang et al., 2004) showing major tectonic subdivisions. (B) Geographic-geological map showing the ophiolite outcrops along the western segment of the YZSZ. (C) Geological sketch map of the Purang ultramafic massif (modified after Liu et al., 2015a). The location of the investigated samples is also shown. YZSZ—Yarlung Zangbo Suture Zone; BNSZ—Bangong–Nujiang Suture Zone; SHSZ—Shuanghu Suture Zone; JSSZ—Jinshajiang Suture Zone; KSZ—Kunlun Suture Zone; N-MORB—normal-type mid-ocean ridge basalt; OIB—ocean island basalt. The yellow circles are sample locations reported from Wei et al. (2006), Liu et al. (2011), Xiong et al. (2011), Bao et al. (2015), and He et al. (2016).**

(UHP) minerals (i.e., diamonds) in the Purang peridotites might imply a deep upper mantle origin for some of these rocks (Yang et al., 2011, 2014; Griffin et al., 2016). Despite these conflicting origins, our present study of mafic intrusions will aid in the resolution of the enigmatic petrogenetic evolution of the Purang ophiolite.

## SAMPLING AND GEOLOGICAL OBSERVATIONS

Our field study was focused on the NW and SE parts of the Purang ultramafic massif (Fig. 1C). A total of 22 samples of mafic intrusions were collected from three well-exposed ultramafic suites to the west of Yungbwa (/Raksas Tal) Lake: (*i*) 30° 32′ N [latitude (φ)], 81° 13′ E [longitude (λ), *N* = 7], (*ii*) 30° 32′ N, 81° 03′ E (*N* = 4), and (*iii*) 30° 42′ N, 80° 43′ E (*N* = 11). Sampling was undertaken to characterize the morphological and petrographic aspects of mafic dikes (to assess their complexity at the cm- to m-scales), and determine if any compositional and isotopic variations exist among them.

The investigated dikes occur as a subtle, but pervasive phenomenon within the Purang mantle suite. They have a pale to dark green color and exhibit an isotropic, fine to medium granular igneous fabric. Dikes in the eastern part of the peridotite massif are less than 1–7 m thick (Figs. 2A, 2B), whereas those in the western part are 10 m thick (Figs. 2C, 2D). They lack distinct modal or textural layering and they do not show lateral ramifications. Each dike appears independent; that is, no dikes were observed to cross cut or connect one to another. The immediate ultramafic host of the dikes is a superficially weathered, sheared, and variably depleted peridotite (Fig. 2A). The contacts between dikes and their host peridotite are generally sharp and planar (Fig. 2B). However, several dikes pre-

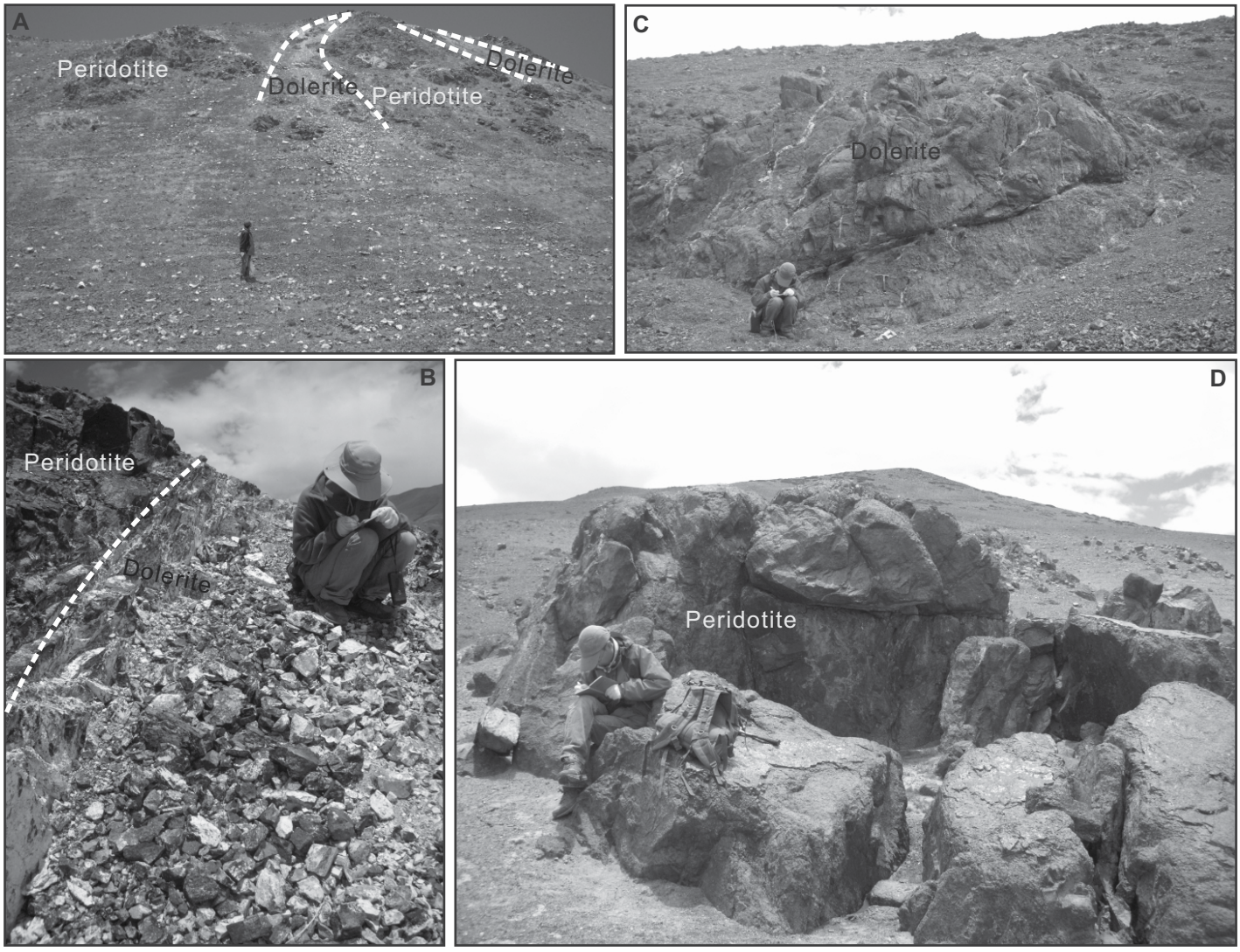


**Figure 2. Field photos showing the mode of occurrence of the dolerite intrusions in the East Purang (A, B) and West Purang (C, D) of the Tibetan Plateau.**

serve chilled margins, implying rapid loss of heat to the host peridotite. Metamorphic aureoles in peridotite comprising the immediate host to the dikes were only occasionally observed. These aureoles are ~1 cm thick, black in color, and made of serpentine ± chlorite.

A structural reconnaissance shows that the distribution of the investigated dikes is rather heterogeneous. Their strike is approximately NW-SE and their dip steep, but quite variable. We note that a number of intrusions cut early asthenospheric fabrics in peridotites (i.e., oriented pyroxene porphyroclasts, spinel strings). Moreover, a few dikes show mylonitic fabrics and boudin structures. These structures represent the effect of semi-ductile shearing on the mafic dikes at an early stage in the life-cycle of the Purang oceanic lithosphere (e.g., Rassios and Dilek, 2009). All mafic intrusions display brittle structures, like streaks and fractures, caused by late reactivation movements during ophiolite emplacement (e.g., Bézard et al., 2011).

Serpentinization and weathering are widespread in the Purang peridotite nappe, but not pervasive. In contrast, rodingitization phenomena are generally scarce. Macroscopic observations confirm that the investigated dikes do not show marks of intense rodingitization.

## PETROGRAPHIC DESCRIPTION

Mafic dikes from the eastern and western part of the Purang peridotite massif show quite similar mineralogical and textural characteristics. Therefore, in this section we will describe them as a single group of mafic rocks, emphasizing their most important petrographic differences when necessary.

Mafic intrusions consist primarily of feldspar and pyroxene. Modal analyses of these rocks average at ~55%–65% plagioclase, 35%–45% clinopyroxene, and trivial amounts of opaque Ti-rich minerals (predominantly ilmenite), permitting their classification as dolerites (Figs. 3A–3D). We note that clinopyroxene within dolerites from West Purang is mainly titanoaugite, whereas clinopyroxene within dolerites from East Purang is augite. Dolerite dikes commonly show an intergranular to intersertal texture (Fig. 3B), where the angular interstices between plagioclase laths are occupied by clinopyroxene granules. However, the thickest dikes contain large clinopyroxene crystals that enclose randomly oriented plagioclase laths, giving rise to a sub-ophitic texture (Fig. 3A). Plagioclase grains have subhedral to euhedral crystal habits, varying in size between 0.05 and 0.30 mm.

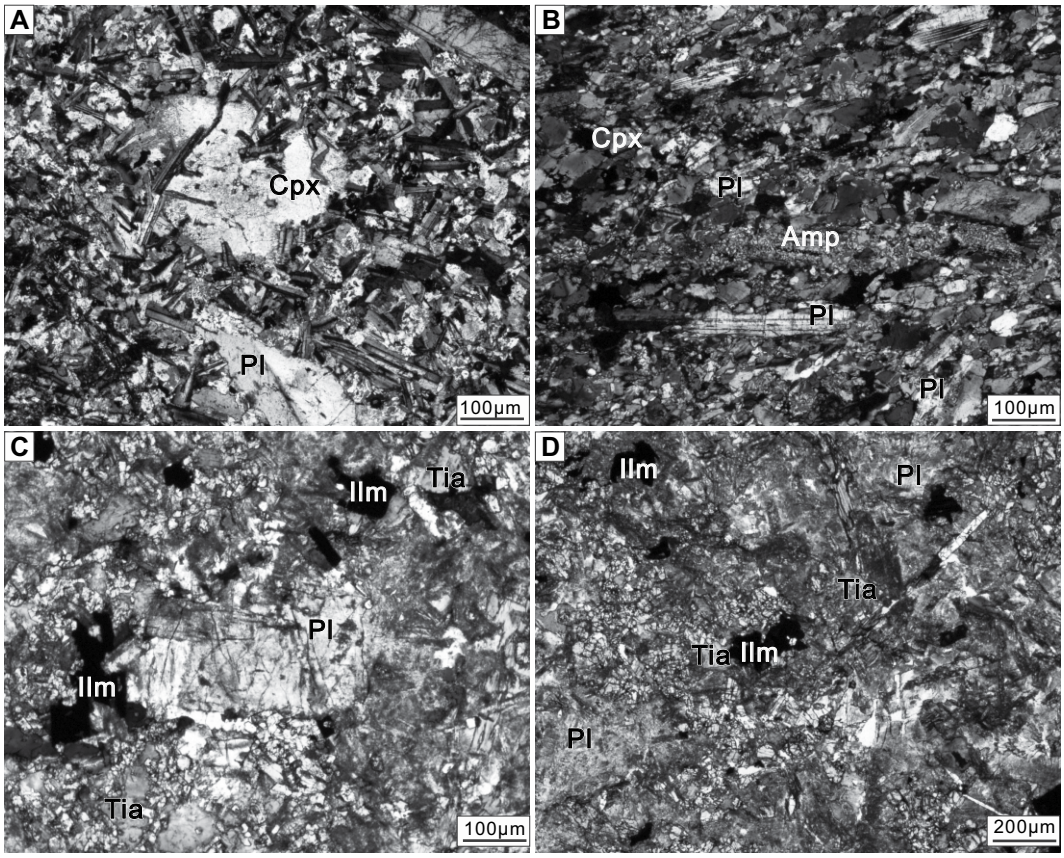


**Figure 3. Photomicrographs of dolerite dikes from the Purang massif of the Tibetan Plateau. Dolerite intrusions within peridotites showing (A) sub-ophitic to ophitic and (B) intergranular to intersertal texture. (C, D) Anidiomorphic to idiomorphic grains of accessory ilmenite between altered plagioclase and titanoaugite crystals. Photos (A) and (B) were taken under crossed polarized transmitted light, whereas photos (C) and (D) were taken under plane polarized transmitted light. Cpx—clinopyroxene; Pl—plagioclase; Amp—amphibole; Ilm—ilmenite; Tia—titano-augite.**

Clinopyroxene forms anhedral to subhedral crystals (≤0.6 mm), showing undulatory extinction. Plagioclase and clinopyroxene crystals are quite often cross cut and offset by brittle compressive fractures. Small (≤100 μm) anidiomorphic to idiomorphic grains of accessory ilmenite occasionally occur dispersed between plagioclase and clinopyroxene crystals (Figs. 3C, 3D).

Dolerite dikes show evidence of post-magmatic alteration. In the altered parts of the investigated dikes, plagioclase is pseudomorphically replaced by sericite and saussurite, and clinopyroxene is replaced by amphibole (tremolite or hornblende) and chlorite. This secondary mineral assemblage is typical of prehnite-pumpellyite to low-grade greenschist facies metamorphism.

Although the study of peridotites is beyond the scope of this paper the main petrographic characteristics of the dike-hosting peridotites from Purang could be summarized as follows: they contain large (0.1–3 mm) porphyroclasts of olivine (~75–80 modal%) and pyroxenes (~20–25 modal%) set in a fine-grained matrix of olivine (±pyroxene) neoblasts, and are classified as harzburgites to lherzolites. Porphyroclasts in these rocks show optical characteristics linked to ductile deformation (i.e., undulatory extinction, tectonic lamellae, and kink bands). Commonly orthopyroxene porphyroclasts show exsolutions of clinopyroxene. Peridotites contain trivial amounts of small (≤0.35 mm) anidiomorphic Cr-spinel and base metal (BM) mineral (i.e., sulfides, alloys) grains. In accordance with our field observations the Purang peridotites are not pervasively serpentinized. Serpentinization is expressed as pseudomorphic serpentine textures (mesh, bastite) typical for altered olivine and pyroxenes. Occasionally, olivine is replaced by iddingsite (a reddish mixture of olivine with clay minerals, chlorite, and Fe-oxyhydroxides) due to superficial weathering.

## ANALYTICAL RESULTS

Samples of dolerite dikes were collected for whole-rock elemental and Sr-Nd isotope analyses, and zircon U-Pb geochronological and Lu-Hf isotope analyses. Details about the analytical methods are given in Data Repository File 1[1], compositional and isotopic data for these samples and standard samples are listed in Data Repository files 2–6.

Consistent with our petrographic observations, the investigated dolerite dikes show low to moderate loss on ignition (LOI) values (1.39–4.89 wt%; Data Repository files 2A, 2B; footnote 1). Nevertheless, major-element oxide concentrations were normalized to 100% on a volatile-free basis to reduce any possible effect of element dilution caused by secondary processes on the investigated dolerites. Therefore, only major and trace elements that are immobile at post-magmatic conditions were used to delineate the geochemistry of the Purang dolerite dikes. These include incompatible elements: Ti, P, Zr, Y, Sc, Nb, Ta, Hf, Th, and middle rare earth elements (MREE), and heavy rare earth elements (HREE), and some transition metals (e.g., Ni, Co, Cr, V). Light REE (LREE) may be mobilized during hydrothermal alteration (e.g.,

[1]GSA Data Repository item 2018404, Supplemental file 1—Laboratory methods; Supplemental file 2a and b—Original major oxides (wt%) and trace elements (ppm) concentrations of dolerites; Supplemental file 3—Whole-rock Sr-Nd isotopic data; Supplemental file 4a—Zircon LA-ICP-MS U-Pb isotopic data; Supplemental file 4b—U-Pb isotopic data of the Standard zircons; Supplemental file 5—Zircon REE data; Supplemental file 6a—Lu-Hf isotopic compositions for zircons; Supplemental file 6b—Lu-Hf isotopic compositions for Standard zircons; Supplemental file 7—References below represent the sources for U-Pb age and Hf-isotope data of zircons from Gangdese Arc plutons and YZSZ ophiolites in Figure 9, is available at http://www.geosociety.org/datarepository/2018 or by request to editing@geosociety.org.

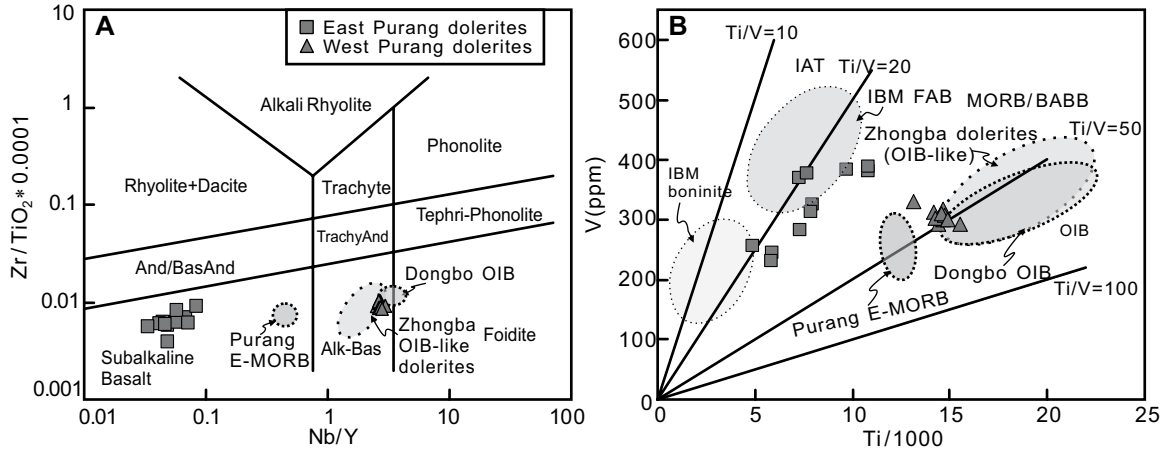


**Figure 4. (A) $Zr/TiO_2*10^{-4}$ vs. Nb/Y (after Winchester and Floyd, 1977) and (B) Vanadium vs. $Ti/10^3$ (after Shervais, 1982) diagrams for the Purang dolerite dikes of the Tibetan Plateau. IBM—Izu-Bonin-Mariana; IAT—island arc tholeiite; OIB—ocean island basalt; FAB—forearc basalt; MORB—mid-ocean ridge basalt; E-MORB—enriched-type mid-ocean ridge basalt; BABB—back-arc basin basalt; BasAnd—basaltic andesite. Data for IBM FAB are from Reagan et al. (2010). Data for the Purang E-MORB and Dongbo OIB are from Liu et al. (2015a), and data for the Zhongba OIB-type dolerites are from He et al. (2016).**

Valsami and Cann, 1992). However, the absence of correlation between LOI and LREE indicates that the later were most likely not affected by post-magmatic processes.

### Major Element Concentrations

Dolerite dikes from East Purang have higher MgO (5.96–7.95 wt%) and CaO (10.42–24.11 wt%) contents than those from the western part of the massif (MgO = 3.15–4.67 wt%, CaO = 5.17–8.57 wt%; Data Repository files 2A, 2B). In contrast, dolerite dikes from East Purang have lower $TiO_2$ (0.81–1.81 wt%), $Na_2O$ (1.66–3.21 wt%), $K_2O$ (0.02–0.18 wt%), and $P_2O_5$ (0.07–0.12 wt%) concentrations compared to those from West Purang ($TiO_2$ = 2.19–2.59 wt%, $Na_2O$ = 3.38–5.58 wt%, $K_2O$ = 0.25–2.36 wt%, $P_2O_5$ = 0.28–0.51 wt%; Data Repository files 2A, 2B). Dolerite intrusions from East Purang have magnesium numbers [$Mg^{\#} = Mg/(Mg + Fe^t) \times 100$] varying between 54 and 66, whereas those from West Purang have $Mg^{\#}$ ranging from 41 to 46.

Based on their plots in the $Zr/TiO_2*10^{-4}$ versus Nd/Y diagram (Winchester and Floyd, 1977) the East Purang dolerite dikes are classified as sub-alkaline rocks, whereas the West Purang dolerite dikes have an alkaline geochemical affinity (Fig. 4A). In the tectonic discrimination diagram of V versus $Ti/10^3$ (Shervais, 1982), the East Purang and West Purang dolerites (Ti/V = 19–28, 40–53, respectively) straddle the boundary between the MORB and island arc tholeiite (IAT) fields and the boundary between the MORB and OIB fields, respectively (Fig. 4B).

### Trace Element Concentrations

The total lanthanide contents of East Purang dolerites range between 29.2 and 54.1 ppm (Data Repository file 2A), analogous to those reported for typical MORB lavas (ΣREE = 39.1 ppm; Sun and McDonough, 1989). The total lanthanide contents of the dolerite dikes from West Purang vary from 199 to 270 ppm (Data Repository file 2B) and are comparable to those reported for OIB-type lavas (ΣREE = 199 ppm; Sun and McDonough, 1989).

The East Purang dolerite dikes are characterized by variable degrees of depletion in the LREE [$(La/Yb)_N$ = 0.62–0.85] and almost flat Gd to Lu segments (Fig. 5A). Several samples display weak negative Eu anomalies, indicating fractionation of plagioclase (Fig. 5A). Such REE distribution patterns correlate well with those of forearc basalts (FAB) from the Izu-Bonin-Mariana trench system (Reagan et al., 2010; Fig. 5A). When plotted in N-MORB–normalized multi-element diagrams, the East Purang dolerite dikes exhibit marked depletions in Nb and Th (Fig. 5B). Furthermore, some samples show slight negative Ti anomalies. The Zr/Nb ratios for this group of dolerites vary from 31 to 77 unlike those of typical N-MORB lavas (not much above 30; Wilson, 1989).

The West Purang dolerite dikes show right-sloping chondrite-normalized REE profiles due to enrichment in the LREE with respect to the HREE [$(La/Yb)_N$ = 13–16; Fig. 5C]. These dolerite dikes show LREE/HREE ratios within the range of those of typical alkaline basalts from the Réunion hotspot in Hawaii (10–11 versus 10–15, respectively; Albarède et al., 1997; Clague et al., 2006). Their N-MORB–normalized spider diagrams resemble those of OIB-type mafic rocks from the Zhongba and Dongbo massifs (Liu et al., 2015a; He et al., 2016; Fig. 5D).

In the tectonic discrimination diagram of Nb*2-Zr/4-Y (Meschede, 1986) the East Purang dolerite dikes plot in the fields of N-MORB lavas and volcanic arc basalts, whereas the West Purang dolerites plot in the field of intra-plate alkaline rocks (Fig. 6A). Furthermore, in the triangular diagram of Y/15-La/10-Nb/8 (Cabanis and Lecolle, 1989) the East Purang dolerites straddle the boundary between the N-MORB and volcanic arc tholeiites (VAT) fields, whereas the West Purang dolerites plot in the field of alkali basalts from intercontinental rifts (Fig. 6B).

We note that previous studies have demonstrated that the dolerite intrusions within the Purang peridotites have N-MORB-normalized multi-element profiles with negative Nb anomalies (e.g., Liu et al., 2011; Xiong et al., 2011; Liu et al., 2013). Our compositional data indicate that this is partly true, since the dolerite dikes cropping out in West Purang do not show negative anomalies in Nb (Fig. 5D).

### Sr-Nd ISOTOPES

The East Purang dolerite dikes have initial $^{87}Sr/^{86}Sr$ ratios (hereafter $^{87}Sr/^{86}Sr_{(i)}$) varying between 0.702953 and 0.70618, and initial $^{143}Nd/^{144}Nd$ ratios (henceforth $^{143}Nd/^{144}Nd_{(i)}$) ranging from 0.51287 to 0.51295. They also show high $\varepsilon_{Nd}(t)$ values, ranging between +7.7 and +9.2 (Data Repository file 3; footnote 1).

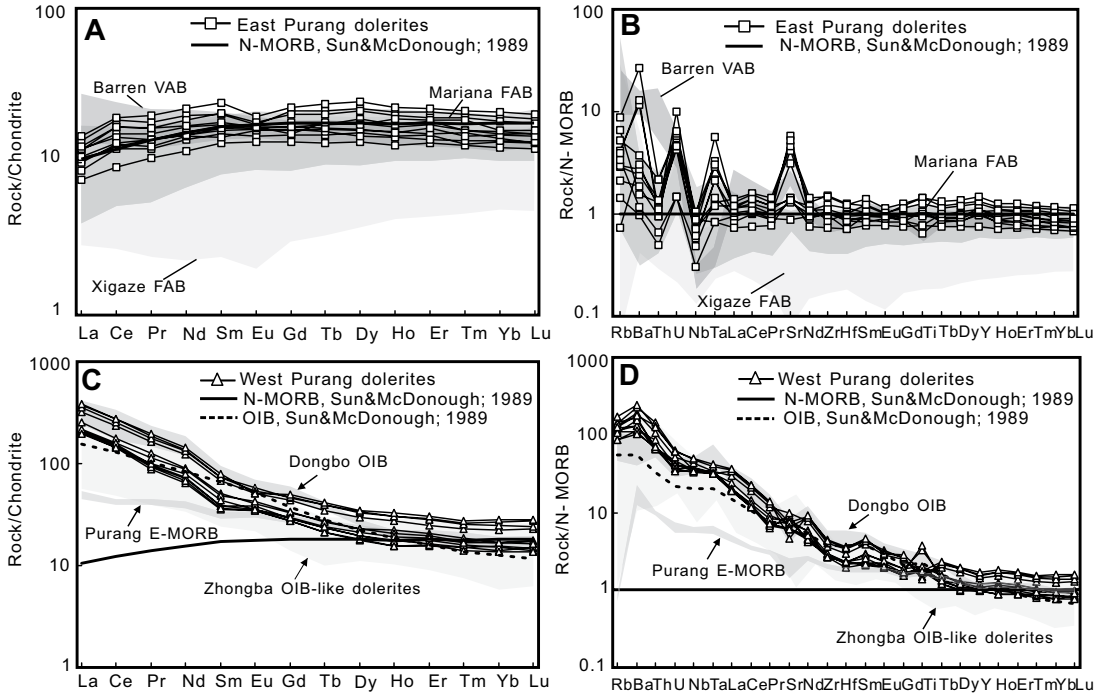


**Figure 5. (A) Chondrite-normalized rare earth element (REE) profiles and (B) normal-type mid-ocean ridge basalt (N-MORB)–normalized multi-element diagrams for the East Purang dolerite dikes of the Tibetan Plateau. (C) Chondrite-normalized REE profiles and (D) N-MORB–normalized multi-element diagrams for the West Purang dolerite dikes. The chondrite, primitive mantle (PM), ocean island basalt (OIB), and N-MORB–normalizing data are from Sun and McDonough (1989). The data for Izu-Bonin-Mariana forearc basalt (FAB), Xigaze FAB, and Barren volcanic arc basalt (VAB) are from Luhr and Haldar (2006), Reagan et al. (2010), and Dai et al. (2013). E-MORB—enriched-type mid-ocean ridge basalt.**

These isotopic compositions are analogous to those previously reported for the dolerite intrusions from Purang ($^{143}Nd/^{144}Nd_{(t)}$ = 0.512904–0.512909, $\varepsilon_{Nd}(t)$ = +8.6 to +8.7; Liu et al., 2013). On the contrary, the West Purang dolerites have quite different isotopic signatures ($^{87}Sr/^{86}Sr_{(i)}$ = 0.70598–0.70765, $^{143}Nd/^{144}Nd_{(i)}$ = 0.51232–0.51234, $\varepsilon_{Nd}(t)$ = –2.6 to –2.3; Data Repository file 3). We also note that the isotopic signatures of these dolerites are quite different compared to those reported for the alkaline basalts from the near Dongbo massif ($^{143}Nd/^{144}Nd_{(t)}$ = 0.512596–0.512630, $\varepsilon_{Nd}(t)$ = +2.6 to +3.3; Liu et al., 2015a).

In the $\varepsilon_{Nd}(t)$ versus $^{87}Sr/^{86}Sr_{(i)}$ binary plot dolerites from East Purang plot within the field of mafic rocks from the YZSZ ophiolites (Fig. 7). In contrast, the West Purang dolerites straddle the boundaries between the fields corresponding to the isotopic compositions of global subducted sediments and OIB lavas (Fig. 7).

## INVESTIGATION OF ZIRCONS

Zircon grains were separated from three dolerite samples (LAC-31, CMN-30, JYM-24). The crystal morphology and internal texture of zircons were studied using optical and scanning electron microscopy prior to isotopic analyses for geochronological dating. To avoid effects of varying experimental conditions each zircon grain was scanned for the same time and back-scattered electron (BSE) and cathodoluminescence (CL) images were taken with constant signal amplification.

### Crystal Morphology and U-Th Contents

Under transmitted light zircons separated from the dolerite sample (LAC-31) are colorless to pale gray and have subhedral prismatic crystal habits. They range in size from 130 × 100 × 80 µm to 70 × 60 × 50 µm. In CL images they show sector to broad-spaced oscillatory zoning parallel to the external faces of the crystals (Fig. 8A). Uranium and Th contents of these zircons vary as follows: 50.8–8068 ppm and 30.4–331 ppm, respectively (Data Repository file 4A; footnote 1). Furthermore, their Th/U ratios range between 0.4 and 1.0.

Zircons separated from the second dolerite sample (CMN-30) are mostly subhedral to ovoid in morphology. Their dimensions range between 130 × 110 × 70 µm and 80 × 70 × 60 µm. Under transmitted light they look dark gray to murky-brown and translucent with a mottled appearance clearly visible in CL images (Fig. 8B). These zircons have low CL signals, but distinctly bright domains are occasionally observed along their crystal boundaries. Furthermore, a few zircon grains display micro-pores possibly due to volume decrease phenomena (e.g., Nasdala et al., 2009). We note that all zircons separated from this sample have quite low interference colors, but normal values of refractive index ($n \geq 1.75$). Moreover, they have high U (83.3–846 ppm) and Th (187–2041 ppm) contents (Data Repository file 4A) as well as high Th/U ratios (0.9–3.3).

Zircons separated from the last dolerite sample (JYM-24) appear as dark to light gray and semi-transparent, columnar to short prismatic grains. Their dimensions range between 200 × 180 × 90 µm and 80 × 70 × 60 µm. These zircons have relatively strong BSE emissions and suppressed CL signals, a common characteristic of several natural zircons that has been described in the literature as "normal" inverse behavior (Corfu et al., 2003). Most zircons recovered from the dolerite sample JYM-24 are practically textureless except for a few grains showing weak oscillatory and irregular

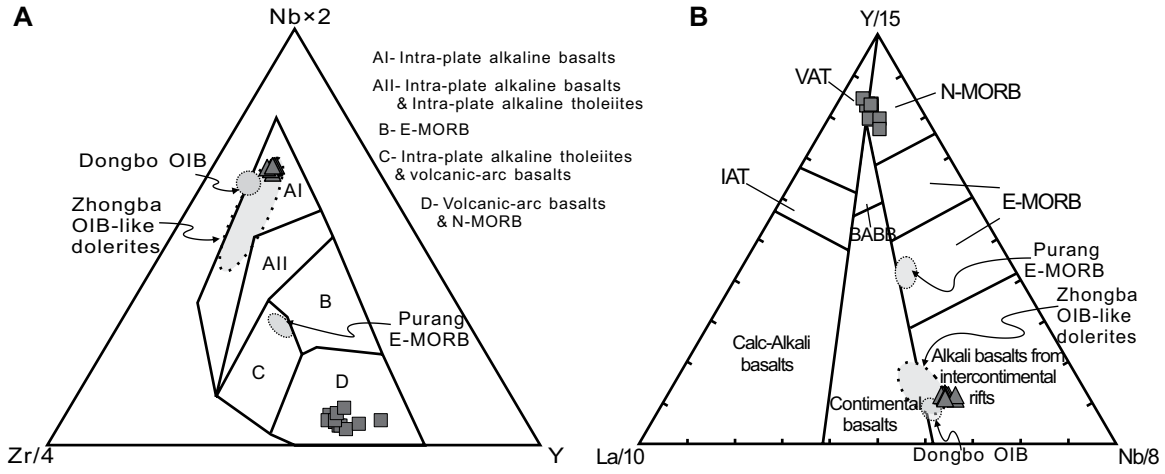


**Figure 6. Tectonic discrimination diagrams for the Purang dolerite dikes of the Tibetan Plateau: (A) Nb*2-Zr/4-Y (after Meschede, 1986); (B) triangular diagram Y/15-La/10-Nb/8 (after Cabanis and Lecolle, 1989). The compositional fields of the Zhongba ocean island basalt (OIB)-type dolerites (He et al., 2016), Dongbo OIB-type mafic rocks, and Purang enriched-type mid-ocean ridge basalt (E-MORB)–type mafic rocks (Liu et al., 2015a) are also shown for comparison. IAT—island arc tholeiite; VAT—volcanic arc tholeiite; N-MORB—normal-type mid-ocean ridge basalt; BABB—back-arc basin basalt.**

internal patterns. We note that the virtual nonluminescence of these zircons in CL images (Fig. 8C) implies high contents of minor and trace elements (particularly U; e.g., Liati and Gebauer, 2009). U and Th contents of zircons are the highest measured herein and show the following variations: 1882–4088 ppm and 2038–7909 ppm, respectively (Data Repository file 4A). The Th/U ratios of these zircons range between 0.9 and 2.6.

All examined zircons are free of visible mineral inclusions and overgrowths; they do not show signs of magmatic resorption or detrital derivation and have no inherited cores. Nevertheless, we note that the investigated zircons display micro-textural and compositional differences, implying that their host dolerite dikes do not share a mutual petrogenetic history.

### Trace Element Composition

The lanthanide contents of zircons separated from the investigated dolerite dikes were normalized to chondrite values (Sun and McDonough, 1989) and plotted on $\log_{10}$ versus trace element (La to Lu) diagrams. The chondrite-normalized REE patterns of zircons separated from the dolerite sample LAC-31 show steep positive slopes from La to Lu with positive Ce anomalies (Fig. 8A). They also show very weak negative Eu anomalies, implying crystallization of zircon before plagioclase (Fig. 8A). Zircons from dolerite sample CMN-30 display enriched in HREE and depleted in LREE chondrite-normalized REE profiles with positive Ce anomalies and marked negative Eu anomalies, suggesting crystallization with plagioclase (Fig. 8B). Zircons from dolerite sample JYM-24 show chondrite-normalized REE profiles with positive slopes from La to Lu, well-expressed positive Ce anomalies and quite strong negative Eu anomalies (Fig. 8C).

The implementation of the Ti-in-zircon geothermometer of Watson et al. (2006) showed that zircons crystallized at a temperature higher than 648 °C. This finding, combined with the high Th/U ratios of the investigated zircons, indicate that they could have crystallized from dike-filling melts. Absence of any significant differences in the REE patterns of zircons separated from a single dolerite dike indicates that the composition of zircons in each dolerite dike was controlled by a single igneous process or a combination of magmatic processes that similarly affected all zircons.

### U-Pb Dating

In a $^{207}Pb/^{235}U$ versus $^{206}Pb/^{238}U$ concordia diagram analyses of 15 zircons separated from dolerite sample LAC-31 and 11 zircons separated from dolerite specimen CMN-30 yielded weighted average $^{206}Pb/^{238}U$ ages of 124.4 ± 3.2 Ma (mean square of weighted deviation, MSWD = 0.34) and 124.5 ± 2.5 Ma (MSWD = 0.10), respectively (Figs. 8A, 8B; Data Reposi-

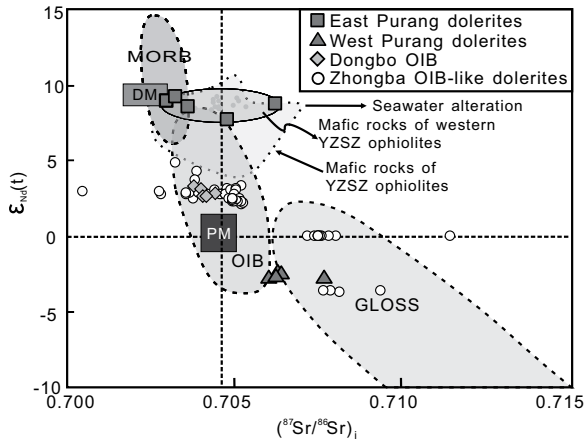


**Figure 7. Binary plot of $\varepsilon_{Nd}(t)$ vs. $^{87}Sr/^{86}Sr_{(i)}$ for the investigated dolerite intrusions of the Tibetan Plateau. Data for the mafic rocks of the Yarlung Zangbo Suture Zone (YZSZ) ophiolites are also shown for comparison (Sources: Aitchison et al., 2000; Miller et al., 2003; Niu et al., 2006; Wang et al., 2006; Zhong et al., 2006; Xia et al., 2008, Xiong et al., 2016; Zhang et al., 2016a; Zhang et al., 2016b; Zheng et al., 2017; Liu et al., 2018). Data for the Zhongba ocean island basalt (OIB)-type dolerites are from He et al. (2016). Data for the Dongbo OIB are from Liu et al. (2015a). MORB—mid-ocean ridge basalt; DM—depleted mantle; PM—primitive mantle; GLOSS—global subducted sediments.**

**Figure 8. Concordia curves of the U-Pb data, insert cathodoluminescence images and chondrite-normalized rare earth element patterns of zircons separated from the dolerite samples (A) LAC31, (B) CMN30, and (C) JYM24 of the Tibetan Plateau. The small solid circles represent sites for the age analysis by laser ablation–inductively coupled plasma–mass spectrometry (LA-ICP-MS), whereas the big dash circles represent the sites for the Lu-Hf isotopic analysis by LA-MC-ICP-MS. N-MORB—normal-type mid-ocean ridge basalt; OIB—ocean island basalt; MSWD—mean standard weighted deviation; conf.—confidence.**

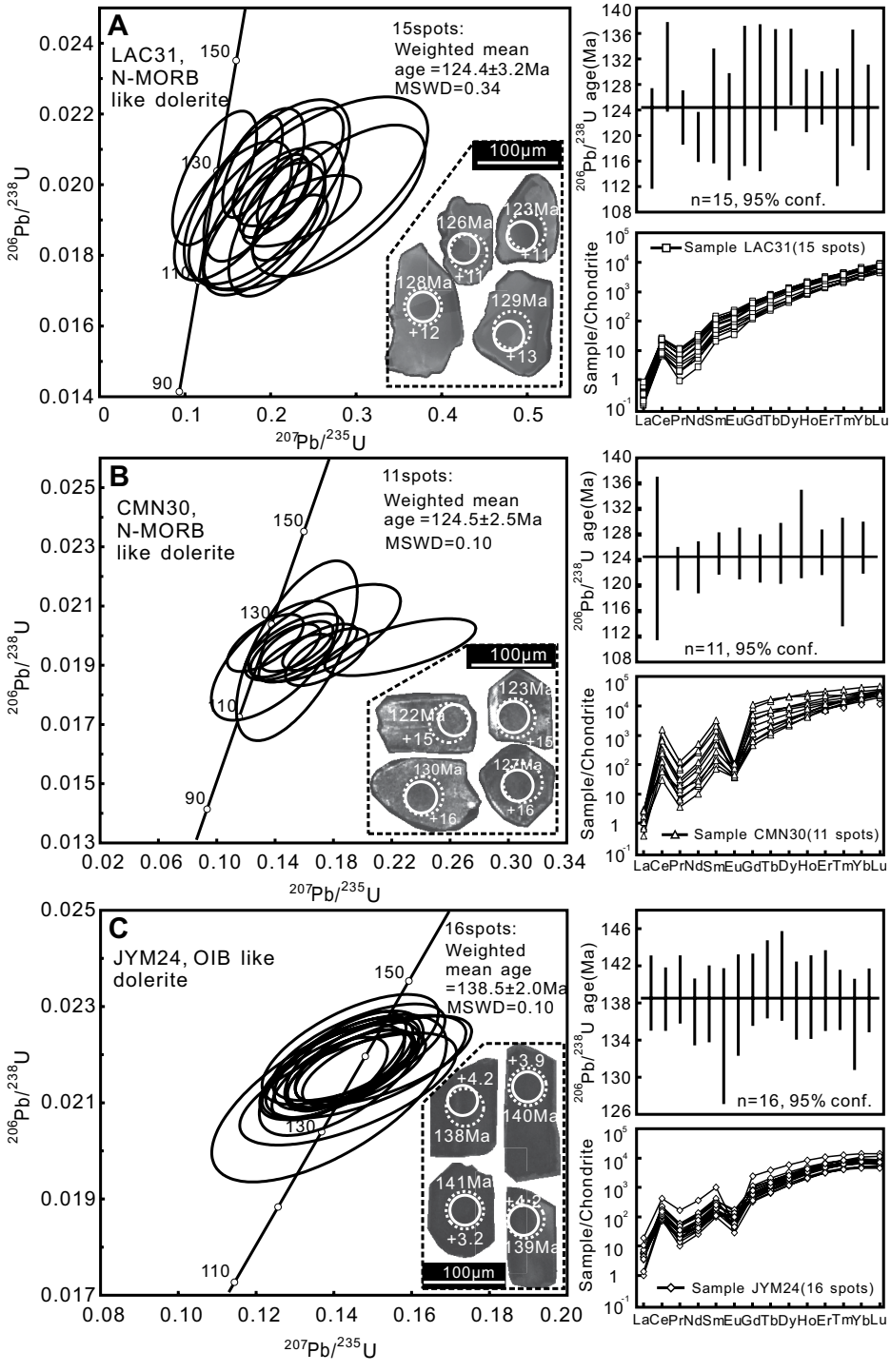


tory file 4A). Most of these data are near-concordant. This is most likely due to common Pb incorporation rather than common Pb loss (e.g., Chew et al., 2014; Spencer et al., 2016). However, the investigated zircons are free of visible mineral inclusions and inherited cores. Furthermore, these zircons do not show evidence of metamictization (/radiation damage). Therefore, it appears that the brittle fractures or resin-related effects lead to the common Pb incorporation.

U-Pb isotopic analyses of 16 zircons separated from dolerite sample JYM-24 form a relatively tight cluster yielding a weighted average $^{206}Pb/^{238}U$ age of 138.5 ± 2.0 Ma (MSWD = 0.10; Fig. 8C).

In accordance with previous studies there is no correlation between U-Pb age and morphology or internal micro-texture of the investigated zircons (e.g., Yamamoto et al., 2013). In addition, the existence of a single zircon age population in each dolerite specimen indicates that all investigated zircons are unlikely of xenocrystic origin.

### Lu-Hf Isotopic Composition and Geochronology

Lu-Hf isotope analyses of zircons were performed on the same spots previously analyzed for U-Pb isotopes. The initial $^{176}Hf/^{177}Hf$ ratios (hereafter $^{176}Hf/^{177}Hf_{(i)}$) of zircons separated from the dolerite sample LAC-31 range between 0.282793 and 0.283111, giving radiogenic $\varepsilon_{Hf}(t)$ values (+3.5 to +14.8, with an average of +9.7). The depleted mantle (DM) Hf model ages ($T_{DM}$) for these zircons vary from 197 Ma to 709 Ma (with an average age of 425 Ma), whereas the "crustal" ($^{C}$) Hf model ages ($T_{DM}^{C}$) vary between 237 Ma and 958 Ma (with an average age of 560 Ma; Data Repository file 6A; footnote 1). Zircons separated from the dolerite sample CMN-30 have $^{176}Hf/^{177}Hf_{(i)}$ values in the range of 0.283051–0.283181. They have a marked mantle Hf-isotopic signature, which is characterized by a relatively tight cluster of positive $\varepsilon_{Hf}(t)$ values (+12.6 to +17.2, with an average of +15.5). Their $\varepsilon_{Hf}(t)$ single stage model ages ($T_{DM}$) are in the range of 88–333 Ma (with an average age of 180 Ma) and their crustal residence ages ($T_{DM}^{C}$) are in the range of 78–374 Ma (with an average age of 191 Ma; Data Repository file 6A). The Lu-Hf isotopic data of zircons separated from dolerite sample JYM-24 yielded $^{176}Hf/^{177}Hf_{(i)}$ values ranging from 0.282762 to 0.282815 and $\varepsilon_{Hf}(t)$ values varying from +2.6 to +4.6 (with an average of +3.5). Their single-stage model ages ($T_{DM}$) and two-stage model ages ($T_{DM}^{C}$) range between 668 Ma and 770 Ma (with an average age of 710 Ma) and from 898 Ma to 1020 Ma (with an average age of 965 Ma), respectively

(Data Repository file 6A). The $\varepsilon_{Hf}(t)$ values of zircons separated from the dolerite sample JYM-24 differ from those of zircons separated from the dolerite samples LAC-31 and CMN-30. We argue that this testifies to the isotopic heterogeneity of the dike-filling melts.

In a probability distribution diagram of U-Pb ages for zircons separated from the Gangdese arc plutons, and mafic dikes and intermediate-felsic granitoids in South Tibet (Xiong et al., 2016; and other references in Data Repository file 7; footnote 1) the ages of zircons separated from the East Purang dolerite dikes are consistent with the widespread mafic magmatism at ca. 130–120 Ma in the YZSZ (Fig. 9A). When plotted against the U-Pb ages of zircons their $\varepsilon_{Hf}(t)$ values show a significant spread, falling between the DM- and chondrite uniform reservoir (CHUR)-control lines (Fig. 9B).

## DISCUSSION

### Possible Effects of Crustal Assimilation, Melt-Peridotite Interaction and Fractional Crystallization

The original composition of an igneous rock might be affected by petrologic processes such as crustal assimilation, melt-mantle interaction, and fractional crystallization to a serious extent (e.g., Liu et al., 2016). Consequently, the effect of such processes on the composition of the Purang dolerite dikes must be discussed in detail before we determine the geochemical characteristics of the mantle sources of their parental magmas.

Dolerites from Purang do not show "topographic" intrusional boundaries and lack (internal) petrographic and compositional layering as for typical cumulate intrusive bodies. They crop out as isolated intrusions within mantle peridotites, precluding any possibility of interaction of the dike-filling melts with crustal rocks. Furthermore, our field and petrographic observations show that the parental melts of dolerites did not interact with the peridotites they encountered en route to lithospheric mantle levels. Some dolerite dikes have chilled margins and cut the shearing planes in peridotites, implying that intrusion of mafic magmas happened at some point after the accretion and ductile deformation of peridotites in a cold lithospheric environment (e.g., Xiong et al., 2016). This environment led to rapid solidification of the dike-filling melts, preventing any kind of metasomatic interaction with ambient peridotites.

The low Cr (21–251 ppm) and Ni (9.09–84.2 ppm) contents of the dolerite dikes from Purang indicate that they were not derived from primitive magmas (e.g., Cr > 400 ppm and Ni > 200 ppm; Tatsumi and Eggins, 1995). The wide range of $Mg^{\#}$ values measured for these mafic dikes (41–66) implies that they originated from variably fractionated melts. Therefore, the effect of magma differentiation on the composition of the investigated mafic intrusions must be determined before any attempt to define the source type of their parental melts.

Positive correlations between Cr, Ni, and $Mg^{\#}$ indicate fractional crystallization of clinopyroxene (Figs. 10A, 10B). The positive correlations between Sc/Y, $CaO/Al_2O_3$, and $Mg^{\#}$ are due to fractionation of clinopyroxene and plagioclase (e.g., Naumann and Geist, 1999; Figs. 10C, 10D). The lack of correlation between $P_2O_5$ and $Mg^{\#}$ is consistent with the absence of apatite in the investigated dolerites (Fig. 10E). Increasing Nb/La ratios with increasing $TiO_2$ concentrations could indicate Fe-Ti oxides in the studied rocks, resulting in high concentrations of high-field-strength elements (HFSE) (Fig. 10I; i.e., Nb, Ta, Zr, and Hf; Klemme et al., 2006; Nielsen and Beard, 2000). However, the negative correlations between FeOt, $TiO_2$, and $Mg^{\#}$ (Figs. 10F, 10G) imply limited fractionation of Fe-Ti oxides in our samples, which is consistent with our petrographic observations. Furthermore, the negative correlation between the Nb/La ratios and $Mg^{\#}$ (Fig. 10H) could not be a result of fractional crystallization or crustal contamination (e.g., Liu et al., 2016). Therefore, the trace element contents of the Purang dolerites were not controlled by cumulus processes and represent liquid compositions. Consequently, we will use incompatible elements (i.e., Ce, Y, Nb, Yb), hygromagmatophile elements (i.e., Th, Ta, Th, Tb), and REE concentrations to decipher the compositional characteristics of the mantle sources of the dike-filling melts. This is because such elements are only slightly affected by fractional crystallization of plagioclase + clinopyroxene (Saccani et al., 2014) and are thought to indicate original geochemical variations in the mantle source (e.g., Allègre and Minster, 1978; Baker et al., 1997).

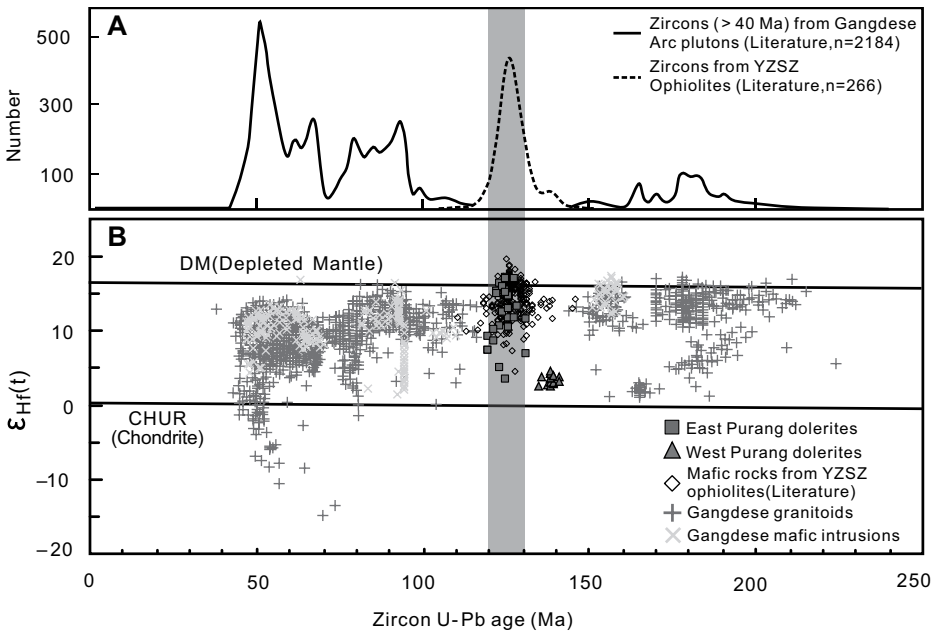


**Figure 9. (A) Probability distribution diagram of U-Pb ages for zircons with $^{206}Pb/^{238}U$ ages >40 Ma from Gangdese Arc plutons, similar mafic intrusions, and intermediate-felsic granitoids of the Tibetan Plateau. (B) Variations of U-Pb ages vs. $\varepsilon_{Hf}(t)$ of zircons separated from the Purang dolerite dikes, similar mafic dikes in the literature, and intermediate-felsic granitoids. Gray column marks the time span of 130–120 Ma. (Data sources, see Data Repository file 7 [footnote 1]). CHUR—chondritic uniform reservoir; YZSZ—Yarlung Zangbo Suture Zone.**

### Mantle Sources and Melting Conditions

In the $TiO_2$/Yb versus Nb/Yb discrimination diagram (Pearce, 2008) our analyses of East Purang dolerite dikes plot in the shallow melting array, showing a similar composition to that of tholeiites derived from melting of depleted MORB mantle (DMM) (Fig. 11). The compositions of dolerites from West Purang straddle the boundary between the fields of OIB and enriched-type mid-ocean ridge basalt (E-MORB), implying that they originated from a deep-seated enriched mantle (EM) source (Fig. 11).

It is known that magmas derived from melting of spinel lherzolite show depleted-in-LREE chondrite-normalized REE patterns (e.g., Work-

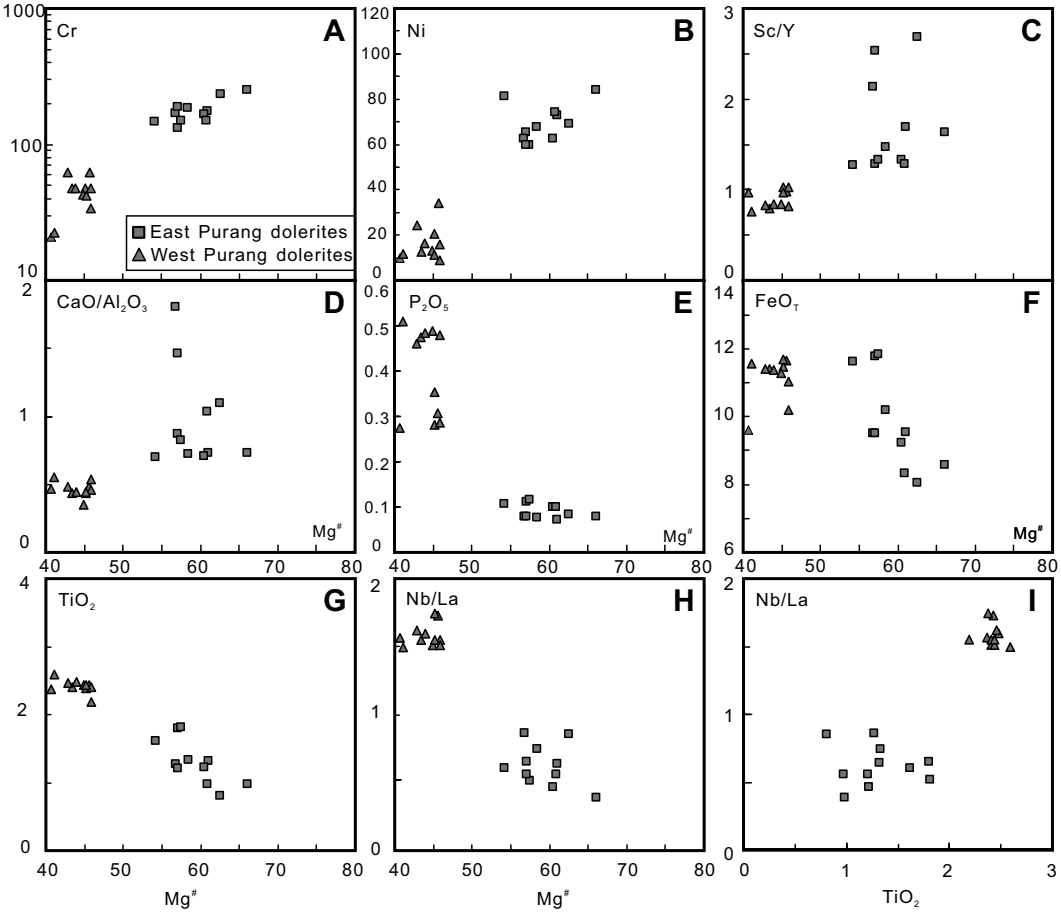


**Figure 10. (A–H) Plots of Cr, Ni, Sc/Y, $CaO/Al_2O_3$, $P_2O_5$, $FeO^t$, $TiO_2$, Nb/La vs. Mg#. (I) Nb/La vs. $TiO_2$ for the Purang dolerite dikes of the Tibetan Plateau.**

man and Hart, 2005), whereas magmas produced by low-degree melting of garnet lherzolite show high fractionation of HREE (e.g., Niu et al., 2002; Saccani et al., 2013a). This seems to explain the origin of the Purang dolerite dike-filling melts. To test the soundness of this hypothesis we applied a non-modal, batch partial melting model using La/Yb versus Dy/Yb ratio plots (Figs. 12A, 12B; Thirlwall et al., 1994). This model illustrates melting curves in garnet- and spinel-facies for two mantle sources ($S_1$ and $S_2$) with compositions analogous to that of DMM (i.e., $Yb_N$ = 2.08; Saccani et al., 2014). The only difference between the two sources is that the first is significantly enriched in LREE, whereas the second is slightly enriched in LREE. The La/Yb and Dy/Yb ratios of dolerites from East Purang can be reproduced by more than 20% melting of lherzolite source $S_2$ in the spinel facies (Fig. 12A). The geochemical signatures of West Purang dolerites cannot be explained by partial melting of the inferred mantle sources in the garnet facies alone. Mixing of variable proportions of magmas derived from melting of an enriched garnet-bearing lherzolite source ($S_1$; ~10 to ≤50 vol%) with melt fractions originating from an enriched spinel-bearing lherzolite source ($S_1$; ~90 to ≥50 vol%) could sufficiently explain the compositions of dolerites (Fig. 12B). For a precise estimation of the degree of melting required for the genesis of the parental magmas of dolerites from West Purang we used the Sm/Yb versus Sm discrimination diagram (Fig. 12C; e.g., Aldanmaz et al., 2000; Pearce, 2008). Our plots show that the parental magmas of these dolerites originated from 5%–10% melting of a lherzolite source containing spinel and garnet at near equal amounts.

We note that the low CaO and high $SiO_2$ contents of dolerites from West Purang contraindicate a pure peridotite source for their parental magmas. It is likely that melting of a "marble cake" mantle region (Allègre and Turcotte, 1986) comprised of peridotite with (ancient) eclogitic/granulitic pyroxenite layers (e.g.,

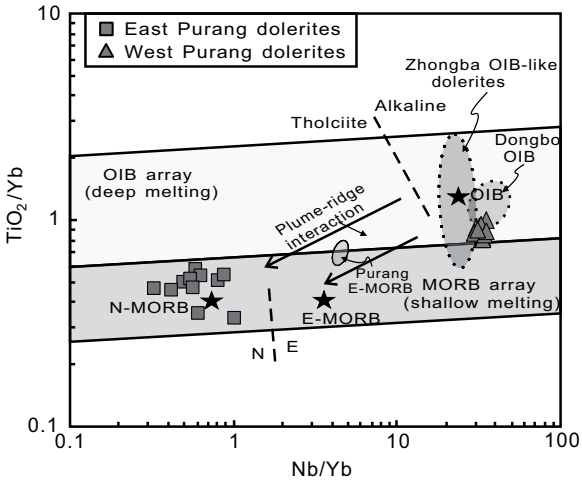


**Figure 11. $TiO_2$/Yb vs. Nb/Yb discrimination diagram (Pearce, 2008) for the Purang dolerite dikes of the Tibetan Plateau. The compositional fields of the Dongbo and Purang alkaline mafic rocks (Liu et al., 2015a) and Zhongba alkaline dolerites (He et al., 2016) are shown for comparison. E-MORB—enriched-type mid-ocean ridge basalt; N-MORB—normal-type mid-ocean ridge basalt; OIB—ocean island basalt.**

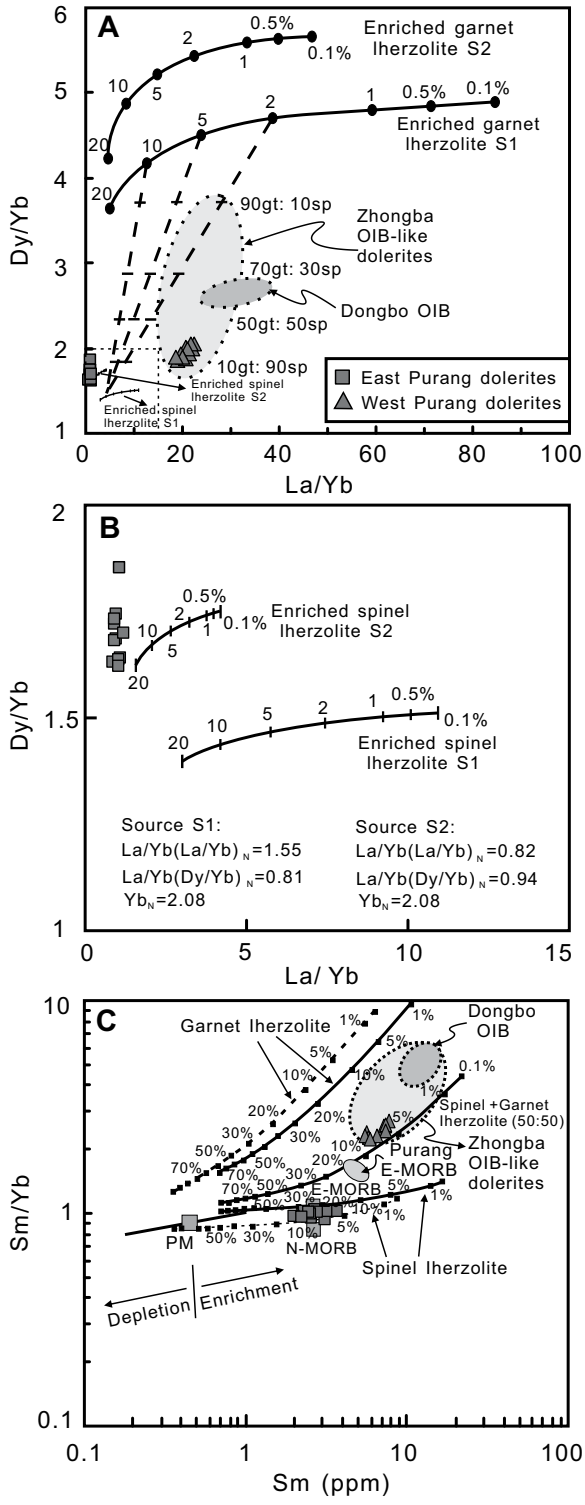


**Figure 12. (A–B) La/Yb vs. Dy/Yb discrimination diagrams for the dolerite dikes from Purang, Tibetan Plateau (after Saccani et al., 2014). Melt curve models based on La/Yb vs. Dy/Yb are calculated using non-modal, batch melts of garnet (gt) and spinel (sp) lherzolites for two different enriched mantle source compositions: $S_1$ (from Saccani et al., 2013a) and $S_2$ (from Saccani et al., 2013b). (A) Melt curves for $S_1$ and $S_2$ in the spinel-facies; (B) melt curves for $S_1$ and $S_2$ in both garnet- and spinel-facies. Arrays representing mixing between various proportions of melt fractions from garnet-facies mantle and melt fractions from spinel-facies mantle are also shown. Garnet lherzolite mode is: 0.598 ol, 0.211 opx, 0.076 cpx, and 0.115 gt that melts in proportions of 0.04 ol, –0.19 opx, 1.04 cpx, and 0.11 gt. Spinel lherzolite mode is: 0.578 ol, 0.270 opx, 0.119 cpx, and 0.033 sp that melts in proportions of –0.06 ol, 0.28 opx, 0.67 cpx, and 0.11 sp. Mantle modes and melting proportions are from Kinzler (1997). Distribution coefficients are from Irving and Frey (1984) for orthopyroxene and clinopyroxene, and from McKenzie and O'Nions (1991) for olivine, spinel, and garnet. Normalizing values are from Sun and McDonough (1989). (C) Sm/Yb versus Sm discrimination diagram for the dolerite dikes from Purang (after Aldanmaz et al., 2000). Numbers on curves denote the degree of partial melting. Melting curves for spinel lherzolite ($ol_{53} + opx_{27} + cpx_{17} + sp_{11}$) and garnet peridotite ($ol_{60} + opx_{20} + cpx_{10} + gt_{10}$), enriched-type mid-ocean ridge basalt (E-MORB), normal-type mid-ocean ridge basalt (N-MORB), and primitive mantle (PM) compositions are after Sun and McDonough (1989). The compositional fields of the Dongbo and Purang alkaline mafic rocks (Liu et al., 2015a) and the Zhongba ocean island basalt (OIB)-type dolerites (He et al., 2016) are also shown for comparison. ol—olivine; opx—orthopyroxene; cpx—clinopyroxene; gt—garnet; sp—spinel.**

Gazel et al., 2011a; Sergeev et al., 2014 and references therein) produced the parental magmas of those dolerites. Interestingly, this interpretation is consistent with the "double distillation" model that was recently proposed to explain the genesis of OIB-type melts (e.g., Mallik and Dasgupta, 2012).

### Evidence for Interaction between MORB-Type Asthenosphere and OIB-Type Components

A magma produced by continuous melting of a single mantle source without becoming mixed with other melts (during its evolution) will follow a curvilinear trend in the Nd versus La diagram (Aldanmaz et al., 2007; Fig. 13A). In this graph the compositions of dolerites from Purang form quasi-linear trends (Fig. 13A), indicating that mixing processes (melt or source mixing, or a combination of both; e.g., Saccani et al., 2014) were probably involved in their formation.

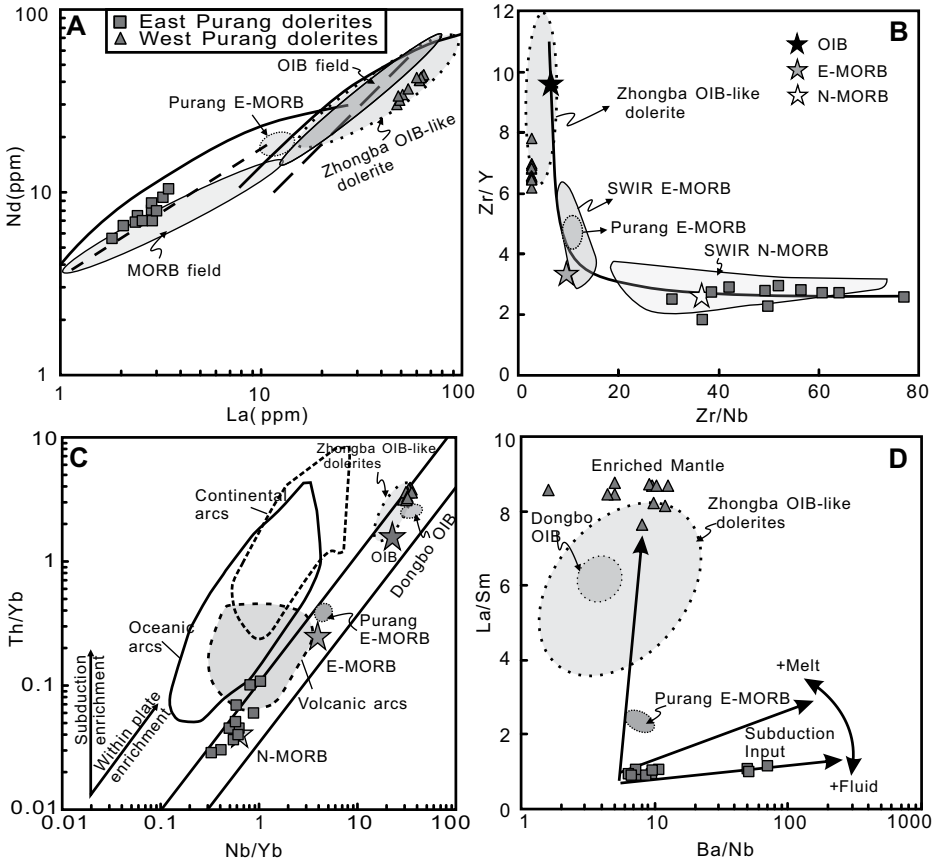


**Figure 13. (A) La vs. Nd plot for the Purang dolerite dikes of the Tibetan Plateau. Curved lines are the expected trends for continuous partial melting of any single mantle source. Dotted lines denote the trends shown by the Zhongba OIB-type dolerites. Linear trends suggest mixing between melts derived from geochemically different magma sources. MORB and OIB fields (shaded regions) are from the Neo-Tethyan ophiolites of West Turkey (Aldanmaz et al., 2007), the Neo-Tethyan ophiolites of the western Yarlung Zangbo Suture Zone (He et al., 2016; Liu et al., 2015a), and the East Pacific Rise (Niu et al., 2002). (B) Zr/Y vs. Zr/Nb diagram for the dolerite dikes from the Purang ultramafic massif (after Saccani et al., 2013a). Stars indicate the compositions of modern OIB, E-MORB, and N-MORB (Sun and McDonough, 1989). The linear trend represents the mixing curve calculated using the OIB and N-MORB endmembers. N-MORB—normal-type mid-ocean ridge basalt; E-MORB—enriched-type mid-ocean ridge basalt; OIB—ocean island basalt. (C) Th/Yb vs. Nb/Yb diagram of Pearce (2008). (D) La/Sm vs. Ba/Nb diagram modified from Escrig et al. (2009). The compositional variations for basalts from the SW Indian Ridge (SWIR) (Le Roex et al., 1983), the Dongbo and Purang alkaline mafic rocks (Liu et al., 2015a), and the Zhongba OIB-type dolerites (He et al., 2016) are also shown for comparison.**

Consequently, the question arises as to what kind of connection exists between MORB- and OIB-type magmatism in the study area. The impact of OIB-type magmatism on typical MORB compositions can be described using the Zr/Y vs. Zr/Nb covariation (Fig. 13B; e.g., Saccani et al., 2013a). In this diagram the compositions of dolerites from East and West Purang seem to follow the mixing curve calculated using N-MORB and OIB endmembers (Sun and McDonough, 1989). This could be linked to melting of a broad MORB-type asthenospheric mantle region containing a decreasing proportion of OIB-type components from deep to shallow mantle levels, rather than magma mixing (e.g., Saccani et al., 2014). We note that OIB-related metasomatism is capable of affecting large areas within the upper mantle (several hundred kilometers in diameter; e.g., Iceland [Magde and Smith, 1995]). This scenario is further corroborated by the recent discovery of E-MOR basalts in the extrusive unit of the Purang ophiolite (Liu et al., 2015a). These rocks were also viewed as products of partial melting of a MORB-type mantle source heterogeneously modified by OIB-type components (Liu et al., 2015a).

Our U-Pb geochronological data indicate that OIB-type magmatism predated MORB-type magmatism in the study area (138.5 Ma versus 124.4 Ma). This is consistent with the eruption age of the E-MORB lavas (137 Ma; Liu et al., 2015a). Consequently, combined data suggest that the supply of OIB-type components in the Purang mantle was decreasing over time.

We note that the intrusion of alkaline dolerite dikes in the West Purang mantle happened in the Early Cretaceous (Valanginian), ~60–100 m.y. later than the incipient continental rifting and opening of the Neo-Tethyan seaway in the study area (Hu et al., 2016). However, the lifespan of a mantle diapir/plume linked to OIB-type magmatism could be greater than 100 Ma (Abers et al., 1988; Kearey et al., 2009), pointing toward a plume-related magmatic activity during the Late Jurassic–Early Cretaceous evolution of the Neo-Tethys (He et al., 2016).

### Evidence for Source Contamination by Crustal Components

Most dolerite analyses plot within the MORB-OIB array in the Th/Yb versus Nb/Yb diagram of Pearce (2008; Fig. 13C). However, a limited number of analyses deviate from this array, showing a slight enrichment in Th/Yb. This indicates that the mantle sources of the dike-filling magmas have been affected by crustal input to a small extent. Consequently, the question arises as to what kind of process caused the inferred crustal input.

### Dolerites from East Purang: Implications for Slab Subduction

The East Purang dolerite intrusions have a higher average Zr/Nb ratio than the whole crust (51 versus 16; Rollinson et al., 2000). They also show apparent negative anomalies in Nb and Th, and some of them show mild negative Ti anomalies in N-MORB–normalized multi-element diagrams, similar to those of tholeiitic magmas derived from arc-related settings (Fig. 5B; Liu et al., 2018). These findings demonstrate that the mantle source of the East Purang dolerite dike-filling melts was enriched by components released from melting of a downgoing lithospheric slab (e.g., Zhao et al., 2013; Dai et al., 2015).

The nature of the medium that transported the inferred components from the subducted slab to the mantle wedge above it needs to be constrained by the study of specific characteristics. It is known that enrichment in fluid-

mobile elements increases the Ba/Nb ratio of a melt, whereas enrichment of in melt-mobile substances results in high La/Sm ratio values (Pearce and Stern, 2006; Escrig et al., 2009). The majority of East Purang dolerites show high Ba/Nb and low La/Sm ratios (Fig. 13D). They also have positive $\varepsilon_{Nd}(t)$ values and high $^{87}Sr/^{86}Sr_{(i)}$ ratios (Fig. 7), implying that their parental magmas were influenced by subduction-related fluids. These fluids aided partial melting of a spinel-bearing mantle source, causing fluid-mobile element enrichment in the resultant mafic melts.

When plotted in the $\varepsilon_{Hf}(t)$ versus U-Pb age diagram analyses of zircons separated from the East Purang dolerites fall between the DM- and CHUR-control lines, suggesting crystallization from magmas derived from a juvenile mantle reservoir (Fig. 9B; e.g., Zlatkin et al., 2014, 2017; Belousova et al., 2015). The wide spread in the $\varepsilon_{Hf}(t)$ values of these zircons (+3.5 to +17.0) indicates that the inferred mantle source was not only geochemically, but also isotopically heterogeneous. We conclude that the genesis of the East Purang dolerite dikes coincides with a period of slab-related igneous activity in south Tibet (~130–120 Ma; e.g., Hébert et al., 2012; Dai et al., 2013; Wu et al., 2014; Griffin et al., 2016; Xiong et al., 2016; Zhang et al., 2016a; Zhang et al., 2016b; Liu et al., 2018; Fig. 9A), representing one of the last "gasps" of ophiolite-related magmatism in the study area.

## Dolerites from West Purang: Implications for Crustal Recycling

Although the West Purang dolerites lack evidence of crustal input, it would be reasonable to assume that subduction-related processes have been involved in their genesis. Below we assess this possibility.

Some West Purang dolerite dikes show slight Hf and Ti negative anomalies (Fig. 5D). However, these anomalies are too weak with respect to those of typical arc-like basalts. The strong enrichment in HFSE shown by this group of dolerite intrusions could be linked to partial melting aided by mantle interaction with adakitic (Kepezhinskas et al., 1996) or slab-derived melts produced by subducted hotspot tracks (i.e., OIB and seamounts; Gazel et al., 2009; Liu et al., 2016). Such melts are capable of crystallizing HFSE-bearing phases, predominantly amphibole (Defant et al., 1992; Sajona et al., 1996). Amphibole-bearing peridotites are known to exist in the study area and have been viewed as a result of refertilization of depleted mantle peridotites by arc-related melts (Liu et al., 2010). Nevertheless, melting of an amphibole-bearing peridotite source would result in a positive correlation between Zr/Nb and Ce/Y (not shown here), and a negative correlation between La/Yb and Dy/Yb (Fig. 12B; Baker et al., 1997; Saccani et al., 2014). This is not the case for the dolerite dikes from West Purang. Furthermore, these dolerites have lower $CaO/Al_2O_3$ ratios (0.35–0.55) than typical alkaline basalts produced by melting of amphibole-bearing mantle (>0.6; Gazel et al., 2011a).

Upwelling of asthenospheric magmas through a slab window with minor contribution from the overlying lithospheric mantle could also explain the high HFSE contents of the dolerite dikes from West Purang (e.g, Reagan and Gill, 1989; Thorkelson et al., 2011). However, these dolerites have high Nb abundances, high $(La/Sm)_{PM}$ ratios, and low $(Sm/Yb)_{PM}$ ratios unlike slab-window basalts (e.g., Gorring and Kay, 2001; Thorkelson et al., 2011). As a result, the investigated dolerites could not have been produced by the leak of OIB-like asthenospheric melts through a delaminated subducted lithospheric slab.

Clearly, slab subduction cannot explain the compositional signatures of dolerites from West Purang. Melting of mantle containing old recycled crustal components has been invoked as an alternative mechanism to explain the genesis of alkaline lithologies with variably high Th/Yb ratios (Fig. 13C; Pearce, 2008). Dolerite intrusions from West Purang contain prismatic zircons with positive $\varepsilon_{Hf}(t)$ values (+2.6 to +4.6; Fig. 9B), indicating that they crystallized from melts derived from a juvenile mantle source. However, the moderate spread in the $\varepsilon_{Hf}(t)$ values combined with the old mean $T^{C}_{DM}$ model ages (ca. 1 Ga) suggests mixing between mantle-derived melts and ancient crustal materials. A wide range of Re-depletion model ages ($T_{RD}$ = 0.1–1.3 Ga) has been reported for the Purang peridotites (Liu et al., 2012; Gong et al., 2016), which is roughly consistent with that reported from other massifs along the YZSZ (Griffin et al., 2016). This time span (0.1–1.3 Ga) implies the existence of an old mantle protolith, which experienced multiple melting events during the Neoproterozoic and Phanerozoic eons. The oldest of those melting events are most likely linked to the Grenville assembly of the Rodinia supercontinent (1.3–0.9 Ga) that caused contamination of the SCLM with subducted crustal components. Consequently, the inferred Grenville-age melt extraction event supports the hypothesis that "polluted" mantle peridotites existed long before the opening of the Neo-Tethys as parts of the SCLM beneath the northern continental margin of Gondwana and served as the platform for the construction of the Upper Jurassic–Early Cretaceous ophiolites of the YZSZ (Gong et al., 2016).

Such findings are not unique to the Tibetan region. We note that the Grenville orogeny is a global-scale Mesoproterozoic–Neoproterozoic (1250–980 Ma) tectono-thermal event that has been recognized in eastern North America, Greenland, Scandinavia, Australia, and South China (e.g., Borg and DePaolo, 1994; Li et al., 2002; Davidson, 2008; Song et al., 2012). Some later events related to the collisional phase of the Grenville orogenic cycle, from ~1000 to ~900 m.y. ago, have also been recognized in East Antarctica, the Eastern Ghats Belt of India, and South China (e.g., Mezger and Cosca, 1999; Boger et al., 2000; Fitzsimons, 2000; Kelly et al., 2002; Li et al., 2006, 2009; Li et al., 2008b; Spencer et al., 2015). Song et al. (2012) suggested the existence of a Grenville orogenic belt along SW China that was most likely united with India and East Antarctica in the Early Neoproterozoic era. In our opinion, the Grenvillian $T^{C}_{DM}$ model ages we found here could be a consequence of the input of old crustal material into the SCLM during the assembly of Gondwana.

## Geotectonic Implications

Ophiolitic rocks with OIB-like geochemical affinities have been reported from the northern and southern belts of the western segment of the YZSZ (e.g., Xia, 1991; Xia and Cao, 1992; Xia and He, 1995; Xia et al., 2008; Zhang et al., 2005; Geng et al., 2010; Bézard et al., 2011; Dai et al., 2012; Liu et al., 2015a; He et al., 2016). The genesis of these rocks has been the subject of many frontline studies and remains a hotly debated issue among geoscientists, many of whom passionately defend hypotheses about their origin.

The OIB-type mafic rocks from the western ophiolitic segment of the YZSZ have been viewed as products of asthenospheric magmatism linked to a slab breakoff event during the Early Cretaceous (Dai et al., 2012). Nevertheless, geochronological data (160.5 Ma; He et al., 2016) show that the OIB-type mafic rocks formed earlier than the inferred slab detachment (130–120 Ma.; Dai et al., 2012). Another model that has been proposed to explain the genesis of the OIB-type mafic rocks from the western YZSZ involves spreading of a back-arc basin (BAB) associated with OIB/seamount recycling (Bézard et al., 2011). However, the geochemical signatures of the mafic rocks intruding the mantle peridotites of the western segment of the YZSZ are significantly different from those of BAB magmas (e.g., Liu et al., 2018).

Previous studies interpreted the OIB-type mafic rocks exposed along the western segment of the YZSZ as a result of a rising mantle plume activity linked to incipient continental rifting

and lithospheric extension (e.g., Xu et al., 2015). In this model a large mantle plume rises from the lower mantle through the mantle transition zone into the upper mantle and becomes emplaced beneath a mature spreading center. The largest igneous provinces (LIP) with OIB-type mafic lithologies, in proximity to the YZSZ, is the Early Cretaceous Comei-Bunbury LIP in the southern Indian Ocean (Zhu et al., 2008, 2009) and the Early Cretaceous Meso-Tethys oceanic plateau in the Bangong Tethys Ocean (Zhang et al., 2014; Lu et al., 2016). However, the OIB-type mafic rocks of both the Comei-Bunbury LIP and the Meso-Tethys oceanic plateau have significantly different geochemical and Sr-Nd isotopic signatures from those of the OIB-type mafic rocks exposed along the YZSZ (Qiu et al., 2010). Consequently, the genesis of the OIB-type lithologies of the YZSZ cannot be linked to the Kerguelen mantle plume.

Direct geologic evidence supporting the existence of a large mantle diapir can be recognized in the west YZSZ, such as: regional doming, anomalous thermal regime, and remnant OIB- or E-MOR-type basaltic "terranes" (Liu et al., 2015a). The small volumes of the OIB-type mafic rocks exposed along the western segment of the YZSZ could be interpreted as an indication of the existence of several small mantle diapirs. However, no significant compositional and Sr-Nd-Pb isotopic differences exist between the alkaline mafic rocks from the northwestern and southwestern belts of the YZSZ (He et al., 2016). Therefore, it is likely that the alkaline mafic rocks from the western YZSZ have been generated from a single mantle plume.

Mantle upwelling associated with plume-influenced rifting could sufficiently explain the coexistence of mafic rocks with OIB- or E-MORB- and N-MORB-like signatures within the Purang ophiolite (e.g., Wendt et al., 1997; Gazel et al., 2009, 2011a,b; Ulrich et al., 2012; Liu et al., 2015a). A similar geochemical makeup has been documented in the Zhongba ophiolite in the central-western part of the YZSZ (Dai et al., 2012). Nevertheless, U-Pb dating of zircons separated from a doleritic rock from the Zhongba massif yielded a concordant age of 160.5 ± 1.3 Ma (MSWD = 0.22, $N$ = 12; He et al., 2016), much older than the West Purang dolerite dikes of this study (138.5 ± 2.0 Ma). This could be a result of episodic magmatism caused by a single mantle plume that could remain active over periods of tens of million years (Abers et al., 1988; Kearey et al., 2009).

We note that the geological, geochemical, and isotopic characteristics of the Purang massif do not resemble those of typical SSZ-like ophiolites nor do they "fit" any existing lithospheric or structural model for MOR-like ophiolites. In a recent work the Purang and Dongbo massifs were interpreted as two Early Cretaceous continental margin-type ophiolites (Liu et al., 2015a). Our data are in support of this scenario. Furthermore, our work demonstrates that the impact of plume-type magmatism was probably decreasing from Dongbo to Purang as a well-developed extrusive unit with OIB-like affinity is missing in Purang.

The alkaline magmatism was followed by a younger phase of tholeiitic magmatism, as indicated by the compositional and geochronological data we collected for the East Purang dolerite dikes. Moreover, specific geochemical and isotopic features of some of those dolerites show that they were generated from melting of a spinel-bearing mantle peridotite source with small input of arc-related fluids during an early stage of subduction in the Early Cretaceous (e.g., Reagan et al., 2010; Whattam and Stern, 2011; Dai et al., 2013). We, therefore, conclude that the parental melts of the tholeiitic dolerites were derived from an asthenospheric source affected by minor slab input when Neo-Tethyan slab subduction was initiated adjacent to a rifted continental margin at ca. 130–120 Ma (e.g., Maffione et al., 2015; Xiong et al., 2016; Zheng et al., 2017; Liu et al., 2018). U-Pb ages (127–124 Ma) and Hf-isotope data ($\varepsilon_{Hf}(t)$ = +7.5 to +17.3) for zircons separated from the tholeiitic dolerite intrusions into the mantle peridotites of the Xigaze ophiolite (central-western YZSZ; Dai et al., 2013) are quite similar to those presented herein (124.4 ± 3.2 Ma and 124.5 ± 2.5 Ma; +3.5 to +17.0). The genesis of these intrusions has also been viewed as a result of seafloor spreading in a forearc setting due to rapid slab rollback during subduction initiation between 130 Ma and 120 Ma (Dai et al., 2013).

## Synthesis

In the Late Jurassic–Early Cretaceous (ca. 150–130 Ma) the Tibetan Neo-Tethyan seaway to the south of Eurasia was separated into two oceanic basins by the (Gondwana-derived) Zhongba-Zhada micro-continent. During this period the ocean floor of the southern basin became strewn with seamounts and continued developing northward due to plume-influenced rifting and ocean seafloor spreading.

Our partial melting models have demonstrated that the parental magmas of the West Purang dolerite dikes were generated from 5%–10% melting of a deep-seated lherzolite source heterogeneously modified by OIB-type components ~138.5 m.y. ago. The genesis of these magmas is envisioned to have occurred in the mantle beneath a spreading ridge-system contaminated by a nearby mantle diapir (Schilling et al., 1985; He et al., 2016) in a way that the melt regime of the ridge system may have entrained or captured "fragments" of the exhumed SCLM beneath the northern continental margin of Gondwana (Liu et al., 2015a; Gong et al., 2016). The presence of an OIB-type extrusive sequence in the Dongbo massif and its absence in Purang could be explained by locating the Purang massif more oceanward relative to the ancient continental margin. This is further corroborated by: (*i*) the lack of plagioclase-bearing peridotites in Purang that could be ascribed to a late-stage refertilization episode and (*ii*) the absence of spatially associated continent-derived extensional allochthons (Gong et al., 2016) typically observed in OCT zones (Manatschal and Müntener, 2009).

Continuous upwelling and melting of a spinel-bearing lherzolite source free of any plume-related components gave rise to MORB-type magmas in the extending Neo-Tethyan seaway to the south of the Zhongba-Zhada micro-continent. However, plate reorganization related to the arrival of the Zhongba-Zhada block at the Gangdese subduction zone in the Early Cretaceous (ca. 130 Ma; Liu et al., 2018 and references therein) provided the geodynamic impetus for a northward intra-oceanic subduction at or near the ridge crest of the inferred oceanic basin. As subduction continued and the Neo-Tethyan lithospheric slab was moving down to greater and hotter depths, the release of hydrous fluids from the top of the slab triggered more than 20% melting of the mantle wedge above it. This process stimulated optimal conditions for the production of juvenile tholeiitic melts with arc-like signatures that intruded the eastern Purang mantle as multiple generations of dolerite dikes (124.4 ± 3.2 Ma, 124.5 ± 2.5 Ma). The intra-oceanic subduction process lasted for at least 5.6 m.y., causing melting events that left variably depleted peridotites (Gao et al., 2015) in the mantle wedge now represented by the Purang ultramafic massif.

Later on, the collision of the trench with the southern margin of the Zhongba-Zhada ribbon continent (ca. 115 Ma; Liu et al., 2018) caused uplift of the arc-trench system resulting in unroofing of depleted peridotites, removal of the thin ophiolitic crust due to erosion and gravity sliding that generated the ophiolitic mélange recognized in the study area.

These processes collectively shaped the petrotectonic architecture of the Purang ophiolite offering an illuminating account of scientific information about the anatomy of the Neo-Tethys in the southwestern Tibet region before this ocean was vanished "once and for all" from the face of the Earth.

## CONCLUDING REMARKS

The present study has led to the following conclusions:

1. Dolerite dikes from the western and eastern parts of the Purang peridotite massif yielded (magmatic) zircon U-Pb ages of ca. 138.5 Ma and ca. 124.5–124.4 Ma, respectively.

2. Dolerite intrusions from West Purang are enriched in HFSE and LREE similar to OIB-type mafic rocks, whereas those from East Purang show N-MORB–like REE patterns with negative Nb and Th (±Ti) anomalies, high $\varepsilon_{Nd}(t)$ values (+7.7 and +9.2), and high $^{87}Sr/^{86}Sr_{(i)}$ (0.702953–0.706184), suggesting an origin from rich-in-fluid arc-type tholeiitic melts.

3. Geochemical modeling shows that the alkaline dolerite dikes derived from 5%–10% melting of a MORB-type mantle source heterogeneously modified by OIB-type components (i.e., old garnet-bearing pyroxenite layers). The tholeiitic dolerite intrusions from East Purang originated from 20% melting of a N-MORB–like mantle source in the spinel stability field.

4. The positive $\varepsilon_{Hf}(t)$ values of the zircons separated from the investigated dolerite dikes imply derivation from juvenile mantle melts. However, the moderate spread in the $\varepsilon_{Hf}(t)$ values of the zircons separated from the West Purang dolerites combined with the old mean $T_{DM}^{C}$ model ages (ca. 1 Ga) suggests mixing between mantle-derived melts and ancient crustal components.

5. A model involving a plume-proximal seafloor-spreading system succeeded by an infant intra-oceanic subduction zone can best explain the compositional and isotopic signatures of the dolerite intrusions within the Purang ultramafic massif.


### ACKNOWLEDGMENTS

We are grateful to Professor Rob Strachan (Science Editor), Professor Fuyuan Wu (Associate Editor), Professor Christopher Spencer, and two anonymous reviewers for their constructive and helpful reviews. We would like to express our gratitude to Professor Kai-Jun Zhang and Professor Guoqing Zhou for their constructive suggestions and Dr. Zhengxin Yin, Dr. Yun Zhong, and Professor Wei Huang for their guidance during the field work. Professor Xianglin Tu and Dr. Liang Li are also greatly thanked for their help at the stage of the geochronological analysis of our samples. This research was funded by the National Natural Science Foundation of China (Nos. 41602231, 41372208, 41402065, and 41472054), National Natural Science Foundation of Guangdong Provience (No.2018B030311030), the China Geological Survey Project (Nos. 1212011121087 and 1212011221088), and the Fundamental Research Funds for the Central Universities of China (grant 171 gpy60). In addition, this study was supported by international program for Ph.D. candidates, Sun Yat-sen University.


### REFERENCES CITED


Abers, G.A., Parsons, B., and Weissel, J.K., 1988, Seamount abundances and distributions in the southeast Pacific: Earth and Planetary Science Letters, v. 87, p. 137–151, https://doi.org/10.1016/0012-821X(88)90070-2.

Aitchison, J.C., Davis, A.M., Liu, J., Luo, H., Malpas, J.G., McDermid, I.R.C., Wu, H., Ziabrev, S.V., and Zhou, M., 2000, Remnants of a Cretaceous intra-oceanic subduction system within the Yarlung-Zangbo suture (southern Tibet): Earth and Planetary Science Letters, v. 183, p. 231–244, https://doi.org/10.1016/S0012-821X(00)00287-9.

Albarède, F., Luais, B., Fitton, G., Semet, M., Kaminski, E., Uptton, B.G.J., Bachèlery, P., and Cheminèe, J.L., 1997, The geochemical regimes of Piton de la Fournaise Volcano (Reunion) during the last 530,000 years: Journal of Petrology, v. 38, p. 171–201, https://doi.org/10.1093/petroj/38.2.171.

Aldanmaz, E., Pearce, J.A., Thirlwall, M.F., and Mitchell, J.G., 2000, Petrogenetic evolution of late Cenozoic, post-collision volcanism in western Anatolia, Turkey: Journal of Volcanology and Geothermal Research, v. 102, p. 67–95, https://doi.org/10.1016/S0377-0273(00)00182-7.

Aldanmaz, E., Yaliniz, M.K., Guçtekin, A., and Goncuoglu, M.C., 2007, Geochemical characteristics of mafic lavas from the Neo Tethyan ophiolites in western Turkey: Implications for heterogeneous source contribution during variable stages of ocean crust generation: Geological Magazine, v. 145, p. 37–54.

Allègre, C.J., and Minster, J.F., 1978, Quantitative models of trace element behaviour in magmatic processes: Earth and Planetary Science Letters, v. 38, p. 1–25, https://doi.org/10.1016/0012-821X(78)90123-1.

Allègre, C.J., and Turcotte, D.L., 1986, Implications of a two-component marble-cake mantle: Nature, v. 323, p. 123–127, https://doi.org/10.1038/323123a0.

Allègre, C.J., Courtillot, V., Tapponnier, P., Hirn, A., Mattauer, M., Coulon, C., Jaeger, J.J., Achache, J., Schärer, U., Marcoux, J., Burg, J.P., Girardeau, J., Armijo, R., Gariépy, C., Göpel, C., Li, T.D., Xiao, X.C., Chang, C.F., Li, G.Q., Lin, B.Y., Teng, J.W., Wang, N.W., Chen, G.M., Han, T.L., Wang, X.B., Deng, W.M., Sheng, H.B., Cao, Y.G., Zhou, J., Qiu, H.R., Bao, P.S., Wang, S.C., Wang, B.X., Zhou, Y.X., and Xu, R.H., 1984, Structure and evolution of the Himalaya-Tibet orogenic belt: Nature, v. 307, p. 17–22, https://doi.org/10.1038/307017a0.

Anonymous, 1972, Penrose field conference on ophiolites: Geotimes, v. 17, p. 24–25.

Baker, J.A., Menzies, M.A., Thirlwall, M.F., and Macpherson, C.G., 1997, Petrogenesis of quaternary intraplate volcanism, Sana'a, Yemen: Implications for plume-lithosphere interaction and polybaric melt hybridization: Journal of Petrology, v. 38, p. 1359–1390, https://doi.org/10.1093/petroj/38.10.1359.

Bao, P.S., Su, L., Wang, J., and Zai, Q.G., 2015, Yarlung Zangbo River Ophiolite [in Chinese]: Beijing, China, Geological Publishing House, 267 p.

Bédard, É., Hébert, R., Guilmette, C., Lesage, G., Wang, C.S., and Dostal, J., 2009, Petrology and geochemistry of the Saga and Sangsang ophiolitic massifs, Yarlung Zangbo Suture Zone, Southern Tibet: Evidence for an arc-back-arc origin: Lithos, v. 113, p. 48–67, https://doi.org/10.1016/j.lithos.2009.01.011.

Bézard, R., Hébert, R., Wang, C., Dostal, J., Dai, J., and Zhong, H., 2011, Petrology and geochemistry of the Xiugugabu ophiolitic massif, western Yarlung Zangbo suture zone, Tibet: Lithos, v. 125, p. 347–367, https://doi.org/10.1016/j.lithos.2011.02.019.

Belousova, E.A., Gonzalez Jimenez, J.M., Graham, I., Griffin, W.L., O'Reilly, S.Y., Pearson, N., Martin, L., Craven, S., and Talavera, C., 2015, The enigma of crustal zircons in upper-mantle rocks: Clues from the Tumut ophiolite, southeast Australia: Geology, v. 43, p. 119–122, https://doi.org/10.1130/G36231.1.

Boger, S.D., Carson, C.J., Wilson, C.J.L., and Fanning, C.M., 2000, Neoproterozoic deformation in the Radok Lake region of the northern Prince Charles Mountains, east Antarctica: Evidence for a single protracted orogenic event: Precambrian Research, v. 104, p. 1–24, https://doi.org/10.1016/S0301-9268(00)00079-6.

Borg, S.G., and DePaolo, D.J., 1994, Laurentia, Australia, and Antarctica as a Late Proterozoic supercontinent: Constraints from isotopic mapping: Geology, v. 22, p. 307–310, https://doi.org/10.1130/0091-7613(1994)022<0307:LAAAAA>2.3.CO;2.

Cabanis, B., and Lecolle, M., 1989, Le diagramme La/10-Y/15-Nb/8 un outil pour la discrimination des series volcaniques et la mise en evidence des processus de mélange et/ou de contamination crustale: Comptes Rendus de l'Academie de Sciences de Paris, v. 309, p. 2023–2029.

Chan, G.H.N., Aitchison, J.C., Crowley, Q.G., Horstwood, M.S.A., Searle, M.P., Parrish, R.R., and Chan, J.S.L., 2015, U-Pb zircon ages for Yarlung Tsangpo suture zone ophiolites, south-western Tibet and their tectonic implications: Gondwana Research, v. 27, p. 719–732, https://doi.org/10.1016/j.gr.2013.06.016.

Chew, D.M., Petrus, J.A., and Kamber, B.S., 2014, U-Pb LAICPMS dating using accessory mineral standards with variable common Pb: Chemical Geology, v. 363, no. 1, p. 185–199, https://doi.org/10.1016/j.chemgeo.2013.11.006.

Chu, M.F., Chung, S.L., Song, B., Liu, D., O'Reilly, S.Y., and Pearson, N.J., 2006, Zircon U-Pb and Hf isotope constraints on the Mesozoic tectonics and crustal evolution of southern Tibet: Geology, v. 34, p. 745–748, https://doi.org/10.1130/G22725.1.

Chu, M.F., Chung, S.L., O'Reilly, S.Y., Pearson, N.J., Wu, F.Y., Li, X.H., Liu, D., Ji, J.Q., Chu, C.H., and Lee, H.Y., 2011, India's hidden inputs to Tibetan orogeny revealed by Hf isotopes of Transhimalayan zircons and host rocks: Earth and Planetary Science Letters, v. 307, p. 479–486, https://doi.org/10.1016/j.epsl.2011.05.020.

Clague, D., Paduan, J., McIntosh, W., Cousens, B., Davis, A., and Reynolds, J., 2006, A submarine perspective of the Honolulu Volcanics, Oahu: Journal of Volcanology and Geothermal Research, v. 151, p. 279–307, https://doi.org/10.1016/j.jvolgeores.2005.07.036.

Corfu, F., Hanchar, J.M., Hoskin, P.W.O., and Kinny, P., 2003, Atlas of zircon textures: Reviews in Mineralogy and Geochemistry, v. 53, p. 469–500, https://doi.org/10.2113/0530469.

Dai, J.G., Wang, C.S., and Li, Y.L., 2012, Relicts of the Early Cretaceous seamounts in the central-western Yarlung Zangbo Suture Zone, southern Tibet: Journal of Asian Earth Sciences, v. 53, p. 25–37, https://doi.org/10.1016/j.jseaes.2011.12.024.

Dai, J.G., Wang, C.S., Polat, A., Santosh, M., Li, Y.L., and Ge, Y.K., 2013, Rapid forearc spreading between 130–120 Ma: Evidence from geochronology and geochemistry of the Xigaze ophiolite, southern Tibet: Lithos, v. 172–173, p. 1–16, https://doi.org/10.1016/j.lithos.2013.03.011.

Dai, J.G., Wang, C.S., Zhu, D.C., Li, Y.L., Zhong, H.T., and Ge, Y.K., 2015, Multi-stage volcanic activities and geodynamic evolution of the Lhasa terrane during the Cretaceous: Insights from the Xigaze forearc basin: Lithos, v. 218–219, p. 127–140, https://doi.org/10.1016/j.lithos.2015.01.019.

Davidson, A., 2008, Late Palaeoproterozoic to mid-Neoproterozoic history of northern Laurentia: An overview of central Rodinia: Precambrian Research, v. 160, p. 5–22, https://doi.org/10.1016/j.precamres.2007.04.023.

Defant, M.J., Jackson, T.E., Drummond, M.S., De Boer, J.Z., Bellon, H., Feigenson, M.D., Maury, R.C., and Stewart, R.H., 1992, The geochemistry of young volcanism throughout western Panama and southeastern Costa Rica: An overview [London]: Journal of the Geological Society, v. 149, p. 569–579, https://doi.org/10.1144/gsjgs.149.4.0569.

Dilek, Y., and Furnes, H., 2011, Ophiolite genesis and global tectonics: Geochemical and tectonic fingerprinting of ancient oceanic lithosphere: Geological Society of America Bulletin, v. 123, p. 387–411, https://doi.org/10.1130/B30446.1.

Dubois-Côté, V., Hebert, R., Dupuis, C., Wang, C.S., Li, Y.L., and Dostal, J., 2005, Petrological and geochemical evidence for the origin of the Yarlung Zangbo ophiolites, southern Tibet: Chemical Geology, v. 214, p. 265–286, https://doi.org/10.1016/j.chemgeo.2004.10.004.

Dupuis, C., Hébert, R., Dubois-Côté, V., Wang, C.S., Li, Y.L., and Li, Z.J., 2005, Petrology and geochemistry of mafic rocks from mélange and flysch units adjacent to the Yarlung Zangbo Suture Zone, southern Tibet: Chemical Geology, v. 214, p. 287–308, https://doi.org/10.1016/j.chemgeo.2004.10.005.

Escrig, S., Bézos, A., Goldstein, S.L., Langmuir, C.H., and Michael, P.J., 2009, Mantle source variations beneath the Eastern Lau spreading center and the nature of subduction components in the Lau basin-Tonga arc system: Geochemistry, Geophysics, Geosystems, v. 10, p. 115–123, https://doi.org/10.1029/2008GC002281.

Feng, G.Y., Yang, J.S., Xiong, F.H., Liu, F., Niu, X.L., Lian, D.Y., Wang, Y.P., and Zhao, Y.J., 2015, Petrology, geochemistry and genesis of the Cuobuzha peridotite in the western Yarlung Zangbo suture zone [in Chinese with English abstract]: Geology in China, v. 42, p. 1337–1353.

Feng, G.Y., Yang, J.S., Dilek, Y., Liu, F., and Xiong, F., 2017, Petrological and Re-Os isotopic constraints on the origin and tectonic setting of the Cuobuzha peridotite, Yarlung Zangbo suture zone, southwest Tibet, China: Lithosphere, v. 10, p. 95–108, https://doi.org/10.1130/L590.1.

Fitzsimons, I.C.W., 2000, Grenville-age basement provinces in East Antarctica: Evidence for three separate collisional orogens: Geology, v. 28, p. 879–882, https://doi.org/10.1130/0091-7613(2000)28<879:GBPIEA>2.0.CO;2.

Gansser, A., 1964, The Geology of the Himalayas: New York, USA, Wiley-Interscience, 289 p.

Gao, J., Yang, J., and Xiong, F., 2015, Podiform chromitites and mantle peridotites of the Purang ophiolite, Western Yarlung-Zangbo suture zone, Tibet: Implications for partial melting and melt-rock interaction in oceanic and subduction-related settings: Acta Geologica Sinica, v. 89, 1 p., https://doi.org/10.1111/1755-6724.12308_10.

Gazel, E., Carr, M.J., Hoernle, K., Feigenson, M.D., Szymanski, D., Hauff, F., and Bogaard, P.V.D., 2009, Galapagos-OIB signature in southern Central America: Mantle refertilization by arc-hot spot interaction: Geochemistry, Geophysics, Geosystems, v. 10, p. 1525–2027, https://doi.org/10.1029/2008GC002246.

Gazel, E., Hoernle, K., Carr, M.J., Herzberg, C., Saginor, I., Bogaard, P.V.D., Hauff, F., Feigenson, M.D., and Swisher, C., III, 2011a, Plume-subduction interaction in southern Central America: Mantle upwelling and slab melting: Lithos, v. 121, p. 117–134, https://doi.org/10.1016/j.lithos.2010.10.008.

Gazel, E., Jr., Abbott, R.N., and Draper, G., 2011b, Garnet-bearing ultramafic rocks from the Dominican Republic: Fossil mantle plume fragments in an ultra high pressure oceanic complex: Lithos, v. 125, p. 393–404, https://doi.org/10.1016/j.lithos.2011.02.021.

Geng, Q.R., Peng, Z.M., and Zhang, Z., 2010, Geochemical study on metamorphosed mafic rocks in ophiolitic zone in the Yarlung Zangpo Great Bend, eastern Tibet, China [in Chinese with English abstract]: Geological Bulletin of China, v. 29, p. 1781–1794.

Girardeau, J., and Mercier, J.C., 1988, Petrology and texture of the ultramafic rocks of the Xigaze ophiolite (Tibet): Constraints for mantle structure beneath slow spreading ridges: Tectonophysics, v. 147, no. 1, p. 33–58, https://doi.org/10.1016/0040-1951(88)90146-1.

Girardeau, J., Mercier, J.C., and Yougong, Z., 1985, Origin of the Xigaze ophiolite, Yarlung Zangbo suture zone, southern Tibet: Tectonophysics, v. 119, no. 1, p. 407–433, https://doi.org/10.1016/0040-1951(85)90048-4.

Gong, X.H., Shi, R.D., Griffin, W.L., Huang, Q.S., Xiong, Q., Chen, S.S., Zhang, M., and O'Reilly, S.Y., 2016, Recycling of ancient subduction-modified mantle domains in the Purang ophiolite (southwestern Tibet): Lithos, v. 262, p. 11–26, https://doi.org/10.1016/j.lithos.2016.06.025.

Gorring, M.L., and Kay, S.M., 2001, Mantle processes and sources of Neogene slab window magmas from southern Patagonia, Argentina: Journal of Petrology, v. 42, no. 6, p. 1067–1094, https://doi.org/10.1093/petrology/42.6.1067.

Griffin, W.L., Afonso, J.C., Belousova, E.A., Gain, S.E., Gong, X.H., González-Jiménez, J.M., Howell, D., Huang, J.X., McGowan, N., Pearson, N.J., Satsukawa, T., Shi, R., Williams, P., Xiong, Q., Yang, J.S., Zhang, M., and O'Reilly, S.Y., 2016, Mantle recycling: Transition zone metamorphism of Tibetan ophiolitic peridotites and its tectonic implications: Journal of Petrology, v. 57, p. 655–684, https://doi.org/10.1093/petrology/egw011.

Harrison, T.M., Yin, A., Grove, M., Lovera, O.M., Ryerson, F.J., and Zhou, X., 2000, The Zedong Window: A record of superposed Tertiary convergence in southeastern Tibet: Journal of Geophysical Research, Solid Earth, v. 105, p. 19211–19230, https://doi.org/10.1029/2000JB900078.

He, J., Li, Y.L., Wang, C.S., Dilek, Y., Wei, Y.S., Chen, X., Hou, Y.L., and Zhou, A., 2016, Plume proximal mid-ocean ridge origin of Zhongba mafic rocks in the western Yarlung Zangbo Suture Zone, Southern Tibet: Journal of Asian Earth Sciences, v. 121, p. 34–55, https://doi.org/10.1016/j.jseaes.2016.01.022.

Hébert, R., Huot, F., Wang, C.S., and Liu, Z.F., 2003, Yarlung Zangbo ophiolites (Southern Tibet) revisited: Geodynamic implications from the mineral record: Geological Society of London, Special Publications, v. 218, p. 165–190, https://doi.org/10.1144/GSL.SP.2003.218.01.10.

Hébert, R., Bezard, R., Guilmette, C., Dostal, J., Wang, C.S., and Liu, Z.F., 2012, The Indus-Yarlung Zangbo ophiolites from Nanga Parbat to Namche Barwa syntaxes, southern Tibet: First synthesis of petrology, geochemistry, and geochronology with incidences on geodynamic reconstructions of Neo-Tethys: Gondwana Research, v. 22, p. 377–397, https://doi.org/10.1016/j.gr.2011.10.013.

Hodges, K.V., 2000, Tectonics of the Himalaya and southern Tibet from two perspectives: Geological Society of America Bulletin, v. 112, p. 324–350, https://doi.org/10.1130/0016-7606(2000)112<324:TOTHAS>2.0.CO;2.

Hu, X.M., Garzanti, E., Wang, J., Huang, W., An, W., and Webb, A., 2016, The timing of India-Asia collision onset-Facts, theories, controversies: Earth-Science Reviews, v. 160, p. 264–299, https://doi.org/10.1016/j.earscirev.2016.07.014.

Huang, G.C., Xu, D.M., Lei, Y.J., and Li, L.J., 2010, Characteristics and geological implications of chert associated with ophiolite in southwestern Tibet [in Chinese with English abstract]: Geology in China, v. 37, no. 1, p. 101–109.

Irving, A.J., and Frey, F.A., 1984, Trace element abundances in megacrysts and their host basalts: Constraints on partition coefficients and megacryst genesis: Geochimica et Cosmochimica Acta, v. 48, p. 1201–1221, https://doi.org/10.1016/0016-7037(84)90056-5.

Ji, W.Q., Wu, F.Y., Chung, S.L., Li, J.X., and Liu, C.Z., 2009, Zircon U-Pb geochronology and Hf isotopic constraints on petrogenesis of the Gangdese batholith, southern Tibet: Chemical Geology, v. 262, p. 229–245, https://doi.org/10.1016/j.chemgeo.2009.01.020.

Kearey, P., Klepeis, K.A., Vine, F.J., and Kearey, P., 2009, Global Tectonics (Third edition): Hoboken, New Jersey, USA, Wiley-Blackwell, 496 p.

Kelly, N.M., Clarke, G.L., and Fanning, C.M., 2002, A two-stage evolution of the Neoproterozoic Rayner Structural Episode: New U–Pb sensitive high resolution ion microprobe constraints from the Oygarden Group, Kemp Land, East Antarctica: Precambrian Research, v. 116, p. 307–330, https://doi.org/10.1016/S0301-9268(02)00028-1.

Kepezhinskas, P., Defant, M.J., and Drummond, M.S., 1996, Progressive enrichment of island arc mantle by melt-peridotite interaction inferred from Kamchatka xenoliths: Geochimica et Cosmochimica Acta, v. 60, p. 1217–1229, https://doi.org/10.1016/0016-7037(96)00001-4.

Kinzler, R.J., 1997, Melting of mantle peridotite at pressures approaching the spinel to garnet transition: Application to mid-ocean ridge basalt petrogenesis: Journal of Geophysical Research. Solid Earth, v. 102, p. 853–874, https://doi.org/10.1029/96JB00988.

Klemme, S., Günther, D., Hametner, K., Prowatke, S., and Zack, T., 2006, The partitioning of trace elements between ilmenite, ulvospinel, armalcolite and silicate melts with implications for the early differentiation of the moon: Chemical Geology, v. 234, p. 251–263, https://doi.org/10.1016/j.chemgeo.2006.05.005.

Le Roex, A.P., Dick, H.J.B., Emrlank, A.J., Reid, A.M., Frey, F.A., and Hart, S.R., 1983, Geochemistry, mineralogy and petrogenesis of lavas erupted along the Southwest Indian Ridge between the Bouvet Triple Junction and 11 degrees East: Journal of Petrology, v. 24, p. 267–318, https://doi.org/10.1093/petrology/24.3.267.

Li, J.F., Xia, B., Liu, L.W., Xu, L.F., He, G.S., Wang, H., Zhang, Y.Q., and Yang, Z.Q., 2008a, SHRIMP U-Pb zircon dating of diabase in the Langa Co ophiolite, Purang, Tibet, China, and its geological significance [in Chinese with English abstract]: Geological Bulletin of China, v. 27, p. 1739–1743.

Li, S.M., Wang, Q., Zhu, D.C., Stern, R.J., Cawood, P.A., Sui, Q.L., and Zhao, Z., 2018, One or two Early Cretaceous arc systems in the Lhasa Terrane, southern Tibet: Journal of Geophysical Research, Solid Earth, v. 123, p. 3391–3413, https://doi.org/10.1002/2018JB015582.

Li, X.H., Li, Z.X., Sinclair, J.A., Li, W.X., and Carter, G., 2006, Revisiting the "Yanbian Terrane": Implications for Neoproterozoic tectonic evolution of the western Yangtze Block, South China: Precambrian Research, v. 151, p. 14–30, https://doi.org/10.1016/j.precamres.2006.07.009.

Li, X.H., Li, W.X., Li, Z.X., Lo, C.H., Wang, J., Ye, M.F., and Yang, Y.H., 2009, Amalgamation between the Yangtze and Cathaysia Blocks in South China: Constraints from SHRIMP U–Pb zircon ages, geochemistry and Nd–Hf isotopes of the Shuangxiwu volcanic rocks: Precambrian Research, v. 174, p. 117–128, https://doi.org/10.1016/j.precamres.2009.07.004.

Li, Z.X., Li, X.H., Zhou, H., and Kinny, P.D., 2002, Grenvillian continental collision in south China: New SHRIMP U–Pb zircon results and implications for the configuration of Rodinia: Geology, v. 30, p. 163–166, https://doi.org/10.1130/0091-7613(2002)030<0163:GCCISC>2.0.CO;2.

Li, Z.X., Bogdanova, S.V., Collins, A.S., Davidson, A., De Waele, B., Ernst, R.E., Fitzsi-mons, I.C.W., Fuck, R.A., Gladkochub, D.P., Jacobs, J., Karlstrom, K.E., Lu, S., Natapov, L.M., Pease, V., Pisarevsky, S.A., Thrane, K., and Vernikovsky, V., 2008b, Assembly, configuration, and break-up history of Rodinia: A synthesis: Precambrian Research, v. 160, p. 179–210, https://doi.org/10.1016/j.precamres.2007.04.021.

Lian, D., Yang, J., Robinson, P.T., Liu, F., Xiong, F., Zhang, L., Gao, J., and Wu, W., 2016, Tectonic evolution of the western Yarlung Zangbo Ophiolitic Belt, Tibet: Implications from the petrology, mineralogy, and geochemistry of the peridotites: The Journal of Geology, v. 124, p. 353–376, https://doi.org/10.1086/685510.

Liati, A., and Gebauer, D., 2009, Crustal origin of zircon in a garnet peridotite: A study of U-Pb SHRIMP dating, mineral inclusions and REE geochemistry (Erzgebirge, Bohemian Massif): European Journal of Mineralogy, v. 21, p. 737–750, https://doi.org/10.1127/0935-1221/2009/0021-1939.

Liu, B., Ma, C.Q., Guo, Y.H., Xiong, F.H., Guo, P., and Zhang, X., 2016, Petrogenesis and tectonic implications of Triassic mafic complexes with MORB/OIB affinities from the western Garzê-Litang ophiolitic mélange, central Tibetan Plateau: Lithos, v. 260, p. 253–267, https://doi.org/10.1016/j.lithos.2016.06.009.

Liu, C.Z., Wu, F.Y., Wilde, S.A., Yu, L.J., and Li, J.L., 2010, Anorthitic plagioclase and pargasitic amphibole in mantle peridotites from the Yungbwa ophiolite (southwestern Tibetan Plateau) formed by hydrous melt metasomatism: Lithos, v. 114, p. 413–422, https://doi.org/10.1016/j.lithos.2009.10.008.

Liu, C.Z., Wu, F.Y., Chu, Z.Y., Ji, W.Q., Yu, L.J., and Li, J.L., 2012, Preservation of ancient Os isotope signatures in the Yungbwa ophiolite (southwestern Tibet) after subduction modification: Journal of Asian Earth Sciences, v. 53, p. 38–50, https://doi.org/10.1016/j.jseaes.2011.08.010.

Liu, C.Z., Zhang, C., Yang, L.Y., Zhang, L.L., Ji, W.Q., and Wu, F.Y., 2014, Formation of gabbronorites in the Purang ophiolite (SW Tibet) through melting of hydrothermally altered mantle along a detachment fault: Lithos, v. 205, p. 127–141, https://doi.org/10.1016/j.lithos.2014.06.019.

Liu, F., Yang, J.S., Chen, S.Y., Li, Z.L., Lian, D.Y., Zhou, W.D., and Zhang, L., 2013, Geochemistry and Sr-Nd-Pb isotopic composition of mafic rocks in the western part of Yarlung Zangbo suture zone: Evidence for intra-oceanic supra-subduction within the Neo-Tethys [in Chinese with English abstract]: Geology in China, v. 40, p. 361–374.

Liu, F., Yang, J.S., Dilek, Y., Xu, Z.Q., Xu, X.Z., Liang, F.H., Chen, S.Y., and Lian, D.Y., 2015a, Geochronology and geochemistry of basaltic lavas in the Dongbo and Purang ophiolites of the Yarlung-Zangbo Suture zone: Plume-influenced continental margin-type oceanic lithosphere in southern Tibet: Gondwana Research, v. 27, p. 701–718, https://doi.org/10.1016/j.gr.2014.08.002.

Liu, F., Yang, J.S., Lian, D.Y., Zhao, H., Zhao, Y.J., and Zhang, L., 2015b, The genesis and tectonic significance of mafic dikes in the western part of the Yarlung Zangbo suture zone, Tibet [in Chinese with English abstract]: Acta Geoscientica Sinica, v. 36, p. 441–454.

Liu, F., Dilek, Y., Xie, Y.-X., Yang, J.-S., and Lian, D.-Y., 2018, Melt evolution of upper mantle peridotites and mafic dikes in the northern ophiolite belt of the Western Yarlung Zangbo suture zone (southern Tibet): Lithosphere, v. 10, p. 109–132, https://doi.org/10.1130/L689.1.

Liu, Z., Li, Y., Xiong, F.H., Wu, D., and Liu, F., 2011, Petrology and geochronology of MOR gabbro in the Purang ophiolite of western Tibet, China [in Chinese with English abstract]: Yanshi Xuebao, v. 27, p. 3169–3279.

Lu, L., Yan, L.L., Li, Q.H., Zeng, L., Jin, X., Zhang, Y.X., Hou, Q.L., and Zhang, K.J., 2016, Oceanic plateau and its significance on the Earth system: A review [in Chinese with English abstract]: Yanshi Xuebao, v. 32, p. 1851–1876.

Luhr, J.F., and Haldar, D., 2006, Barren Island Volcano (NE Indian Ocean): Island-arc high alumina basalts produced by troctolite contamination: Journal of Volcanology and Geothermal Research, v. 149, p. 177–212, https://doi.org/10.1016/j.jvolgeores.2005.06.003.

Maffione, M., Van Hinsbergen, D.J.J., Koornneef, L., Guilmette, C., Hodges, K.V., Huang, W., Kapp, P., and Ding, L., 2015, Forearc hyperextension dismembered the South Tibetan ophiolites: Geology, v. 43, no. 6, p. 475–478, https://doi.org/10.1130/G36472.1.

Magde, L.S., and Smith, D.K., 1995, Seamount volcanoes at the Reykjanes ridge: Relationship to the Iceland hotspot: Journal of Geophysical Research. Solid Earth, v. 100, p. 8449–8468, https://doi.org/10.1029/95JB00048.

Mallik, A., and Dasgupta, R., 2012, Reaction between MORB-eclogite derived melts and fertile peridotite and generation of ocean island basalts: Earth and Planetary Science Letters, v. 329–330, p. 97–108.

Manatschal, G., and Müntener, O., 2009, A type sequence across an ancient magma-poor ocean continent transition: the example of the western Alpine Tethys ophiolites: Tectonophysics, v. 473, p. 4–19.

McGowan, N., Griffin, W.L., Gonzalez-Jimenez, J.M., Belousova, E.A., Afonso, J.C., Shi, R., McCammon, C., Pearson, N.J., and O'Reilly, S.Y., 2015, Tibetan chromitites: Excavating the slab graveyard: Geology, v. 43, p. 179–182, https://doi.org/10.1130/G36245.1.

McKenzie, D., and O'Nions, R.K., 1991, Partial melt distributions from inversion of rare earth element concentrations: Journal of Petrology, v. 32, p. 1021–1091, https://doi.org/10.1093/petrology/32.5.1021.

Meschede, M., 1986, A method of discriminating between different types of mid-ocean ridge basalts and continental tholeiites with the Nb-Zr-Y diagram: Chemical Geology, v. 56, p. 207–218, https://doi.org/10.1016/0009-2541(86)90004-5.

Mezger, K., and Cosca, M.A., 1999, The thermal history of the Eastern Ghats Belt (India) as revealed by U-Pb and 40Ar/39Ar dating of metamorphic and magmatic minerals: Implications for the SWEAT correlation: Precambrian Research, v. 94, p. 251–271, https://doi.org/10.1016/S0301-9268(98)00118-1.

Miller, C., Thöni, M., Framk, W., Schuster, R., Melcher, F., Meisel, T., and Zanetti, A., 2003, Geochemistry of tectonomagmatic affinity of the Yungbwa ophiolite, SW Tibet: Lithos, v. 66, p. 155–172, https://doi.org/10.1016/S0024-4937(02)00217-7.

Moores, E.M., Kellogg, L.H., and Dilek, Y., 2000, Tethyan ophiolites, mantle convection, and tectonic "historical contingency": A resolution of the "ophiolite conundrum", *in* Dilek, Y., Moores, E.M., Elthon, D., and Nicolas, A., eds., Ophiolites and oceanic crust: New insights from field studies and the Ocean Drilling Program: Geological Society of America Special Paper 349, p. 3–12, https://doi.org/10.1130/0-8137-2349-3.3.

Nasdala, L., Kronz, A., Wirth, R., Váczi, T., Pérez-Soba, C., Willner, A., and Kennedy, A.K., 2009, The phenomenon of deficient electron microprobe totals in radiation-damaged and altered zircon: Geochimica et Cosmochimica Acta, v. 73, p. 1637–1650, https://doi.org/10.1016/j.gca.2008.12.010.

Naumann, T.R., and Geist, D.J., 1999, Generation of alkalic basalt by crystal fractionation of tholeiitic magma: Geology, v. 27, p. 423–426, https://doi.org/10.1130/0091-7613(1999)027<0423:GOABBC>2.3.CO;2.

Nicolas, A., Girardeau, J., Marcoux, J., Dupré, B., Wang, X., Cao, Y., Zheng, H., and Xiao, X., 1981, The Xigaze ophiolite (Tibet): A peculiar oceanic lithosphere: Nature, v. 294, p. 414–417, https://doi.org/10.1038/294414a0.

Nielsen, R.L., and Beard, J.S., 2000, Magnetite-melt HFSE partitioning: Chemical Geology, v. 164, p. 21–34, https://doi.org/10.1016/S0009-2541(99)00139-4.

Niu, X.L., Zhao, Z.D., Mo, X.X., Depaolo, D.J., Dong, G.C., Zhang, S.Q., et al., 2006, Elemental and Sr-Nd-Pb isotopic geochemistry for basic rocks from Decun-Angren ophiolites in Xigaze area, Tibet: Implications for the characteristics of the Tethyan upper mantle domain [in Chinese with English abstract]: Yanshi Xuebao, v. 22, p. 2875–2888.

Niu, Y., Regelous, M., Wendt, I.J., Batiza, R., and O'Hara, M.J., 2002, Geochemistry of near-EPR seamounts: Importance of source vs. process and the origin of enriched mantle component: Earth and Planetary Science Letters, v. 199, p. 327–345, https://doi.org/10.1016/S0012-821X(02)00591-5.

Pearce, J.A., 2008, Geochemical fingerprinting of oceanic basalts with applications to ophiolite classification and the search for Archean oceanic crust: Lithos, v. 100, p. 14–48, https://doi.org/10.1016/j.lithos.2007.06.016.

Pearce, J.A., and Deng, W.M., 1988, The ophiolites of the Tibetan geotraverses, Lhasa to Golmud (1985) and Lhasa to Kathmandu (1986): Philosophical Transactions of the Royal Society A. Mathematical, Physical and Engineering Sciences, v. 327, no. 1594, p. 215–238, https://doi.org/10.1098/rsta.1988.0127.

Pearce, J.A., and Stern, R.J., 2006, Origin of back-arc basin magmas: Trace element and isotope perspectives, *in* Christie, D.M., Fisher, C.R., Lee, S-M., and Givens, S., eds., Back-Arc Spreading Systems: Geological, Biological, Chemical, and Physical Interactions: Washington D.C., USA, American Geophysical Union: Geophysical Monograph Series, v. 166, p. 63–86.

Qiu, B.B., Zhu, D.C., Zhao, Z.D., and Wang, L.Q., 2010, The westward extension of Comei fragmented large igneous province in southern Tibet and its implications: Yanshi Xuebao, v. 26, p. 2207–2216.

Rassios, A.E., and Dilek, Y., 2009, Rotational deformation in the Jurassic Mesohellenic ophiolites, Greece, and its tectonic significance: Lithos, v. 108, p. 207–223, https://doi.org/10.1016/j.lithos.2008.09.005.

Reagan, M.K., and Gill, J.B., 1989, Coexisting calcalkaline and high-niobium basalts from Turrialba Volcano, Costa Rica: Implications for residual titanates in arc magma sources: Journal of Geophysical Research, Solid Earth, v. 94, p. 4619–4633, https://doi.org/10.1029/JB094iB04p04619.

Reagan, M.K., Ishizuka, O., Stern, R.J., Kelley, K.A., Ohara, Y., Blichert-Toft, J., Bloomer, S.H., Cash, J., Fryer, P., Hanan, B.B., Hickey-Vargas, R., Ishii, T., Kimura, J.I., Peate, D.W., Rowe, M., and Woods, M., 2010, Fore-arc basalts and subduction initiation in the Izu-Bonin-Mariana system: Geochemistry, Geophysics, Geosystems, v. 11, p. 1–17, https://doi.org/10.1029/2009GC002871.

Rollinson, H.R., Yang, X.M., Yang, X.Y., and Chen, S.X., 2000, Lithogeochemistry [in Chinese]: Hefei, China, University of Science and Technology of China Press, 275 p.

Saccani, E., Allahyari, K., Beccaluva, L., and Bianchini, G., 2013a, Geochemistry and petrology of the Kermanshah ophiolite (Iran): Implication for the interaction between passive rifting, oceanic accretion, and OIB-type components in the Southern Neo-Tethys Ocean: Gondwana Research, v. 24, p. 392–411, https://doi.org/10.1016/j.gr.2012.10.009.

Saccani, E., Azimzadeh, Z., Dilek, Y., and Jahangiri, A., 2013b, Geochronology and petrology of the Early Carboniferous Misho Mafic Complex (NW Iran), and implications for the melt evolution of Paleo-Tethyan rifting in Western Cimmeria: Lithos, v. 162–163, p. 264–278.

Saccani, E., Allahyari, K., and Rahimzadeh, B., 2014, Petrology and geochemistry of mafic magmatic rocks from the Sarve-Abad ophiolites (Kurdistan region, Iran): Evidence for interaction between MORB-type asthenosphere and OIB-type components in the southern Neo-Tethys Ocean: Tectonophysics, v. 621, p. 132–147, https://doi.org/10.1016/j.tecto.2014.02.011.

Sajona, F.G., Maury, R.C., Bellon, H., Cotten, J., and Defant, M., 1996, High field strength element enrichment of Pliocene–Pleistocene island arc basalts, Zamboanga peninsula, western Mindanao (Philippines): Journal of Petrology, v. 37, p. 693–726, https://doi.org/10.1093/petrology/37.3.693.

Schilling, J.G., Thompson, G., Kingsley, R., and Humphris, S., 1985, Hotspot-migrating ridge interaction in the South Atlantic: Nature, v. 313, no. 5999, p. 187–191, https://doi.org/10.1038/313187a0.

Searle, M.P., Cooper, D.J.W., Rex, A.J., and Colchen, M., 1988, Tectonic evolution of the Himalayas and Tibet-collision tectonics of the Ladakh-Zanskar Himalaya: Philosophical Transactions of the Royal Society of London, v. 326, p. 117–150, https://doi.org/10.1098/rsta.1988.0082.

Sergeev, D.S., Dijkstra, A.H., Meisel, T., Brügmann, G., and Sergeev, S.A., 2014, Traces of ancient mafic layers in the Tethys oceanic mantle: Earth and Planetary Science Letters, v. 389, p. 155–166, https://doi.org/10.1016/j.epsl.2013.10.039.

Shervais, J.W., 1982, Ti-V plots and the petrogenesis of modern and ophiolitic lavas: Earth and Planetary Science Letters, v. 59, p. 101–118, https://doi.org/10.1016/0012-821X(82)90120-0.

Song, S., Su, L., Li, X.-H., Niu, Y., and Zhang, L., 2012, Grenville-age orogenesis in the Qaidam-Qilian block: The link between South China and Tarim: Precambrian Research, v. 220–221, p. 9–22, https://doi.org/10.1016/j.precamres.2012.07.007.

Spencer, C.J., Cawood, P.A., Hawkesworth, C.J., Prave, A.R., Roberts, N.M.W., Horstwood, M.S.A., and Whitehouse, M.J., 2015, Generation and preservation of continental crust in the Grenville Orogeny: Geoscience Frontiers, v. 6, no. 3, p. 357–372, https://doi.org/10.1016/j.gsf.2014.12.001.

Spencer, C., Kirkland, C., and Taylor, R., 2016, Strategies towards statistically robust interpretations of in situ U–Pb zircon geochronology: Geoscience Frontiers, v. 7, no. 4, p. 581–589, https://doi.org/10.1016/j.gsf.2015.11.006.

Su, B.X., Teng, F.Z., Hu, Y., Shi, R.D., Zhou, M.F., Zhu, B., Liu, F., Gong, X.H., Huang, Q.S., Xiao, Y., Chen, C., and He, Y.S., 2015, Iron and magnesium isotope fractionation in oceanic lithosphere and sub-arc mantle: Perspectives from ophiolites: Earth and Planetary Science Letters, v. 430, p. 523–532, https://doi.org/10.1016/j.epsl.2015.08.020.

Sun, S.S., and McDonough, W.F., 1989, Chemical and isotopic systematics of oceanic basalts: Implications for mantle composition and processes, in Saunders, A.D., and Norry, M.J., eds., Magmatism in the Ocean Basins: Geological Society of London, Special Publications, v. 42, p. 313–345, https://doi.org/10.1144/GSL.SP.1989.042.01.19.

Tatsumi, Y., and Eggins, S.M., 1995, Subduction Zone Magmatism: Cambridge, UK, Blackwell, 211 p.

Thirlwall, M.F., Smith, T.E., Graham, A.M., Theodorou, N., Hollings, P., Davidson, J.P., and Arculus, R.J., 1994, High field strength element anomalies in arc lavas: Source or process: Journal of Petrology, v. 35, p. 819–838, https://doi.org/10.1093/petrology/35.3.819.

Thorkelson, D.J., Madsen, J.K., and Sluggett, C.L., 2011, Mantle flow through the Northern Cordilleran slab window revealed by volcanic geochemistry: Geology, v. 39, p. 267–270, https://doi.org/10.1130/G31522.1.

Ulrich, M., Hémond, C., Nonnotte, P., and Jochum, K.P., 2012, OIB/seamount recycling as an alternative process for E-MORB genesis: Geochemistry, Geophysics, Geosystems, v. 13, no. 6, p. 96–109, https://doi.org/10.1029/2012GC004078.

Valsami, E., and Cann, J.R., 1992, Mobility of rare earth elements in zones of intense hydrothermal alteration in the Pindos ophiolite, Greece: Geological Society of London, Special Publications, v. 60, p. 219–232, https://doi.org/10.1144/GSL.SP.1992.060.01.13.

Wang, C.S., Liu, Z.F., and Hébert, R., 2000, The Yarlung-Zangbo paleo-ophiolite, southern Tibet: Implications for the dynamic evolution of the Yarlung-Zangbo Suture Zone: Journal of Asian Earth Sciences, v. 18, no. 6, p. 651–661, https://doi.org/10.1016/S1367-9120(00)00033-X.

Wang, R., Xia, B., Hu, J.R., Zhou, G.Q., Wei, D.L., and Wang, X.B., 2006, Geochemistry of oceanic island diabase from ophiolitic mélange zone in Renbu area: Implications for hotspot within Tethys in southern Xizang (Tibet) [in Chinese with English abstract.]: Geochimica, v. 35, p. 41–54.

Watson, E.B., Wark, D.A., and Thomas, J.B., 2006, Crystallization thermometers for zircon and rutile: Contributions to Mineralogy and Petrology, v. 151, p. 413–433, https://doi.org/10.1007/s00410-006-0068-5.

Wei, Z.Q., Xia, B., Zhang, Y.Q., and Wang, R., 2006, SHRIMP zircon dating of diabase in the Xiugugabu ophiolite in Tibet and its geological implications [in Chinese with English abstract]: Geotectonica et Metallogenia, v. 30, p. 93–97.

Wen, D.R., Liu, D., Chung, S.L., Chu, M.F., Ji, J., Zhang, Q., Song, B., Lee, T.Y., Yeh, M.W., and Lo, C.H., 2008, Zircon SHRIMP U-Pb ages of the Gangdese Batholith and implications for Neotethyan subduction in southern Tibet: Chemical Geology, v. 252, p. 191–201, https://doi.org/10.1016/j.chemgeo.2008.03.003.

Wendt, J.I., Regelous, M., Collerson, K.D., and Ewart, A., 1997, Evidence for a contribution from two mantle plumes to island-arc lavas from northern Tonga: Geology, v. 25, p. 611–614, https://doi.org/10.1130/0091-7613(1997)025<0611:EFACFT>2.3.CO;2.

Whattam, S.A., and Stern, R.J., 2011, The 'subduction initiation rule': A key for linking ophiolites, intra-oceanic forearcs, and subduction initiation: Contributions to Mineralogy and Petrology, v. 162, no. 5, p. 1031–1045, https://doi.org/10.1007/s00410-011-0638-z.

Wilson, M.B., 1989, Igneous Petrogenesis: A Global Tectonic Approach: Dordrecht, The Netherlands, Springer, 466 p., https://doi.org/10.1007/978-1-4020-6788-4.

Winchester, J.A., and Floyd, P.A., 1977, Geochemical discrimination of different magma series and their differentiation products using immobile elements: Chemical Geology, v. 20, p. 325–343, https://doi.org/10.1016/0009-2541(77)90057-2.

Workman, R.K., and Hart, S.R., 2005, Major and trace element composition of the depleted MORB mantle (DMM): Earth and Planetary Science Letters, v. 231, p. 53–72, https://doi.org/10.1016/j.epsl.2004.12.005.

Wu, F.Y., Liu, C.Z., Zhang, L.L., Zhang, C., Wang, J.G., Ji, W.Q., and Liu, X.C., 2014, Yarlung Zangbo ophiolite: A critical updated view [in Chinese with English abstract]: Yanshi Xuebao, v. 30, p. 293–325.

Xia, B., 1991, The characteristic of rock geochemistry and origin for Laangco ophiolite in Tibet [in Chinese with English abstract]: Geology in Tibet, v. 1, p. 38–54.

Xia, B., and Cao, Y.G., 1992, The Gongzhucuo ophiolite and its tectonic environment in Tibet [in Chinese with English abstract]: Geology in Tibet, v. 2, p. 11–29.

Xia, B., and He, M.Y., 1995, Petrogeochemistry and genetic significance of the Jianapeng ophiolite Tibet [in Chinese with English abstract]: Acta Mineralogica Sinica, v. 15, no. 2, p. 236–241.

Xia, B., Chen, G.W., Wang, R., and Wang, Q., 2008, Seamount volcanism associated with the Xigaze ophiolite, Southern Tibet: Journal of Asian Earth Sciences, v. 32, p. 396–405, https://doi.org/10.1016/j.jseaes.2007.11.008.

Xiong, F., Yang, J., Xua, X., Kapsiotis, A., Hao, X., and Liu, F., 2018, Compositional and isotopic heterogeneities in the Neo-Tethyan upper mantle recorded by coexisting Al-rich and Cr-rich chromitites in the Purang peridotite massif, SW Tibet (China): Journal of Asian Earth Sciences, v. 159, p. 109–129, https://doi.org/10.1016/j.jseaes.2018.03.024.

Xiong, F.H., Yang, J.S., Liang, F.H., Ba, D.Z., Zhang, J., Xu, X.Z., Li, Y., and Liu, Z., 2011, Zircon U-Pb ages of the Dongbo ophiolite in the western Yarlung Zangbo suture zone and their geological significance [in Chinese with English abstract]: Yanshi Xuebao, v. 27, p. 3223–3238.

Xiong, Q., Griffin, W.L., Zheng, J., O'Reilly, S.Y., Pearson, N.J., Xu, B., and Belousova, E.A., 2016, Southward trench migration at ~130–120 Ma caused accretion of the Neo-Tethyan forearc lithosphere in Tibetan ophiolites: Earth and Planetary Science Letters, v. 438, p. 57–65, https://doi.org/10.1016/j.epsl.2016.01.014.

Xu, D.M., Huang, G.C., and Lei, Y.J., 2008, Geochemistry and tectonic significance of mantle peridotites from the Laangcuo ophiolite massif, southwest Tibet [in Chinese with English Abstract]: Acta Petrological et Mineralogical, v. 27, p. 1–13.

Xu, X.Z., Yang, J.S.,Guo, G.L., and Li, J.Y., 2011, Lithological research on the Purang mantle peridotite in western Yarlung-Zangbo suture zone in Tibet: Acta Petrologica Sinica, v. 27, p. 3179–3196 (in Chinese with English abstract).

Xu, Z.Q., Dilek, Y., Yang, J.S., Liang, F.H., Liu, F., Cai, Z.H., Li, G.W., Dong, H.W., and Ji, S.C., 2015, Crustal structure of the Indus-Tsangpo suture zone and its ophiolites in southern Tibet: Gondwana Research, v. 27, p. 507–524, https://doi.org/10.1016/j.gr.2014.08.001.

Yamamoto, S., Komiya, T., Yamamoto, H., Kaneko, Y., Terabayashi, M., Katayama, I., Iizuka, T., Maruyama, S., Yang, J., and Kon, Y., 2013, Recycled crustal zircons from podiform chromitites in the Luobusa ophiolite, southern Tibet: The Island Arc, v. 22, p. 89–103, https://doi.org/10.1111/iar.12011.

Yang, J.S., Dobrzhinetskaya, L., Bai, W.J., Fang, Q.S., Robinson, P.T., Zhang, J., and Green, H., 2007, Diamond and coesite-bearing chromitites from the Luobusa ophiolite, Tibet: Geology, v. 35, p. 875–878, https://doi.org/10.1130/G23766A.1.

Yang, J.S., Xu, X.Z., Li, Y., Li, J.Y., Ba, D.Z., Rong, H., and Zhang, Z.M., 2011, Diamonds recovered from peridotite of the Purang ophiolite in the Yarlung-Zangbo suture of Tibet: A proposal for a new type of diamond occurrence [in Chinese with English abstract]: Yanshi Xuebao, v. 27, no. 11, p. 3171–3178.

Yang, J.S., Xu, X.Z., Bai, W.J., Zhang, Z.M., and Rong, H., 2014, Features of diamond in ophiolite [in Chinese with English abstract]: Yanshi Xuebao, v. 30, no. 8, p. 2113–2124.

Zhang, C., Liu, C.Z., Wu, F.Y., Zhang, L.L., and Ji, W.Q., 2016a, Geochemistry and geochronology of mafic rocks from the Luobusa ophiolite, South Tibet: Lithos, v. 245, p. 93–108, https://doi.org/10.1016/j.lithos.2015.06.031.

Zhang, K.J., Xia, B.D., Wang, G.M., Li, Y.T., and Ye, H.F., 2004, Early Cretaceous stratigraphy, depositional environments, sandstone provenance, and tectonic setting of central Tibet, western China: Geological Society of America Bulletin, v. 116, p. 1202–1222, https://doi.org/10.1130/B25388.1.

Zhang, K.J., Xia, B., Zhang, Y.X., Liu, W.L., Zeng, L., Li, J.F., and Xu, L.F., 2014, Central Tibetan Meso-Tethyan oceanic plateau: Lithos, v. 210–211, p. 278–288, https://doi.org/10.1016/j.lithos.2014.09.004.

Zhang, L.L., Liu, C.Z., Wu, F.Y., Zhang, C., Ji, W.Q., and Wang, J.G., 2016b, Sr–Nd–Hf isotopes of the intrusive rocks in the Cretaceous Xigaze ophiolite, southern Tibet: Constraints on its formation setting: Lithos, v. 258–259, p. 133–148, https://doi.org/10.1016/j.lithos.2016.04.026.

Zhang, S.Q., Mahoney, J.J., Mo, X.X., Ghazi, A.M., Milani, L., Crawford, A.J., Guo, T.Y., and Zhao, Z.D., 2005, Evidence for a widespread Tethyan upper mantle with Indian Ocean-type isotopic characteristics: Journal of Petrology, v. 46, p. 829–858, https://doi.org/10.1093/petrology/egi002.

Zhao, Z.F., Dai, L.Q., and Zheng, Y.F., 2013, Postcollisional mafic igneous rocks record crust-mantle interaction during continental deep subduction: Scientific Reports, v. 3, no. 3413, https://doi.org/10.1038/srep03413.

Zheng, H., Huang, Q., Kapsiotis, A., Xia, B., Yin, Z., Zhong, Y., Lu, Y., and Shi, X., 2017, Early Cretaceous ophiolites of the Yarlung Zangbo suture zone: Insights from dolerites and peridotites from the Baer upper mantle suite, SW Tibet (China): International Geology Review, v. 59, no. 11, p. 1471–1489, https://doi.org/10.1080/00206814.2016.1276867.

Zhong, L.F., Xia, B., Zhou, G.Q., Wang, R., Wei, D.L., and Li, J.F., 2006, Origin of the Luobusa ophiolite, southern Tibet: Sr-Nd-Pb isotopic constraints on crust lavas [in Chinese with English abstract.]: Journal of Mineralogy and Petrology, v. 26, p. 57–63.

Zhou, M.F., Robinson, P.T., Malpas, J., and Li, Z., 1996, Podiform chromitites from the Luobusa ophiolite (southern Tibet): Implications for melt/rock interaction and chromite segregation in the upper mantle: Journal of Petrology, v. 37, p. 3–21, https://doi.org/10.1093/petrology/37.1.3.

Zhou, M.F., Robinson, P.T., Malpas, J., Edwards, S.J., and Qi, L., 2005, REE and PGE geochemical constraints on the formation of dunites in the Luobusa ophiolite, southern Tibet: Journal of Petrology, v. 46, p. 615–639, https://doi.org/10.1093/petrology/egh091.

Zhu, D., Mo, X., Pan, G., Zhao, Z., Dong, G., Shi, Y., Liao, Z., Wang, L., and Zhou, C., 2008, Petrogenesis of the earliest Early Cretaceous mafic rocks from the Cona area of the eastern Tethyan Himalaya in south Tibet: Interaction between the incubating Kerguelen plume and the eastern Greater India lithosphere?: Lithos, v. 100, p. 147–173, https://doi.org/10.1016/j.lithos.2007.06.024.

Zhu, D.C., Chung, S.L., Mo, X.X., Zhao, Z.D., Niu, Y., Song, B., and Yang, Y.H., 2009, The 132 Ma Comei-Bunbury large igneous province: Remnants identified in present day southeastern Tibet and southwestern Australia: Geology, v. 37, p. 583–586, https://doi.org/10.1130/G30001A.1.

Zlatkin, O., Avigad, D., and Gerdes, A., 2014, Peri-Amazonian provenance of the Proto-Pelagonian basement (Greece), from zircon U-Pb geochronology and Lu-Hf isotopic geochemistry: Lithos, v. 184, p. 379–392, https://doi.org/10.1016/j.lithos.2013.11.010.

Zlatkin, O., Avigad, D., and Gerdes, A., 2017, The Pelagonian terrane of Greece in the peri-Gondwanan mosaic of the Eastern Mediterranean: Implications for the geological evolution of Avalonia: Precambrian Research, v. 290, p. 163–183, https://doi.org/10.1016/j.precamres.2017.01.005.

Manuscript Accepted 28 October 2018